Tectonic control on southern Sierra Nevada topography, California

Gweltaz Mahéo,[1] Jason Saleeby,[2] Zorka Saleeby,[2] and Kenneth A. Farley[2]

Received 11 June 2008; revised 1 June 2009; accepted 13 August 2009; published 5 December 2009.

[1] In this study we integrate the apatite (U-Th)/He thermochronometric technique with geomorphic, structural, and stratigraphic studies to pursue the origin and evolution of topographic relief related to extensive late Cenozoic faulting in the southern Sierra Nevada. The geomorphology of this region reflects a transition from a vast region to the north characterized by nonequilibrium fluvial modification of a relict low-relief landscape, little affected by internal deformation, to a more complex landscape affected by numerous faults. Regionally, the relict landscape surface is readily resolved by age-elevation relationships of apatite He ages coupled to geomorphology. These relationships can be extended into the study area and used as a structural datum for the resolution of fault offsets and related tilting. On the basis of 63 new apatite He ages and stratigraphic data from proximal parts of the San Joaquin basin we resolve two sets of normal faults oriented approximately N–S and approximately NW. Quaternary west-side-up normal faulting along the N–S Breckenridge–Kern Canyon zone has resulted in a southwest step over from the Owens Valley system in the controlling structure on the regional west tilt of Sierran basement. This zone has also served as a transfer structure partitioning Neogene-Quaternary extension resulting from normal displacements on the NW fault set. This fault system for the most part nucleated along Late Cretaceous structures with late Cenozoic remobilization representing passive extension by oblate flattening as the region rose and stretched in response to the passage of a slab window and the ensuing delamination of the mantle lithosphere from beneath the region. **Citation:** Mahéo, G., J. Saleeby, Z. Saleeby, and K. A. Farley (2009), Tectonic control on southern Sierra Nevada topography, California, *Tectonics*, *28*, TC6006, doi:10.1029/2008TC002340.

1. Introduction

[2] The evolution of topographic relief is controlled by tectonics, climate, lithologic contrasts, and sedimentary/volcanic fluxes. When these factors are stable topographic relief reaches a steady state whereby perturbations in uplift or erosion rates, or lithologic competency will alter relief toward a new steady state. In intensively studied cases of river profiles adjusting to tectonic perturbations, the characteristic channel adjustment time is estimated to be less than a million years, depending on the basin area [*Whipple and Tucker*, 1999; *Whipple*, 2001; *Snyder et al.*, 2000]. Thus initial relief will evolve through time and produce areas characterized by inherited or paleotopography. Numerous techniques based on field studies, and both numerical and analog models have been developed to reconstruct relief and landscape evolution (see *Burbank and Anderson* [2000] for a review). Field studies are usually based on the reconstruction of the initial relief and comparison with the present-day morphology constraining the landscape evolution. Recent developments in low temperature thermochronology (apatite (U-Th)/He and fission track methods) provide new tools to study relief evolution [(*Stüwe et al.*, 1994; *Mancktelow and Grasemann*, 1997; *House et al.*, 1998; *Braun*, 2002]. The use of low temperature thermochronology is based on the fact that the isothermal surfaces dated by apatite (U-Th)/He and fission track methods (~75°C and ~120°C respectively [*Farley*, 2000; *Gallagher et al.*, 1998]) are higher beneath crests and ridges, and lower beneath valleys [*Stüwe et al.*, 1994; *Mancktelow and Grasemann*, 1997; *House et al.*, 1998; *Braun*, 2002]. Thus these techniques are sensitive to both the geomorphology and to the wavelength and amplitude of its evolutionary changes.

[3] In this study we develop an additional application of the apatite He technique to the origin and evolution of topographic relief in an extensively faulted region. In the case of a steady state thermal structure with planar and horizontal isotherms, in a region where little deformation has occurred, samples collected at the same elevation should have the same age for a given thermochronometer. If deformation occurred after the cooling of the samples then the age distribution can be used to reconstruct the structural relief of folding, faulting or tilting [cf. *Wolf et al.*, 1996]. This technique is useful in areas where geomorphic or stratigraphic features that can be used as paleohorizontal references are lacking. This is especially true in expansive exposures of crystalline basement. Among the different low temperature thermochronometers the apatite He system is particularly useful in that (1) low temperature isotherms are usually not affected by subsolidus regime cooling of granitic bodies which at higher temperatures produce complex thermal structures and (2) it provides the youngest possible ages of exhumation and thus the closest to the development of the studied landform, which reduces the possibility that the observed age pattern has resulted from successive erosional or tectonic events [*Farley*, 2002].

[1]Laboratoire des Sciences de la Terre, UMR 5570, Université de Lyon, Ecole Normale Supérieure de Lyon, Université Claude Bernard Lyon 1, CNRS, Villeurbanne, France.
[2]Division of Geological and Planetary Sciences, California Institute of Technology, Pasadena, California, USA.

0278-7407/09/2008TC002340

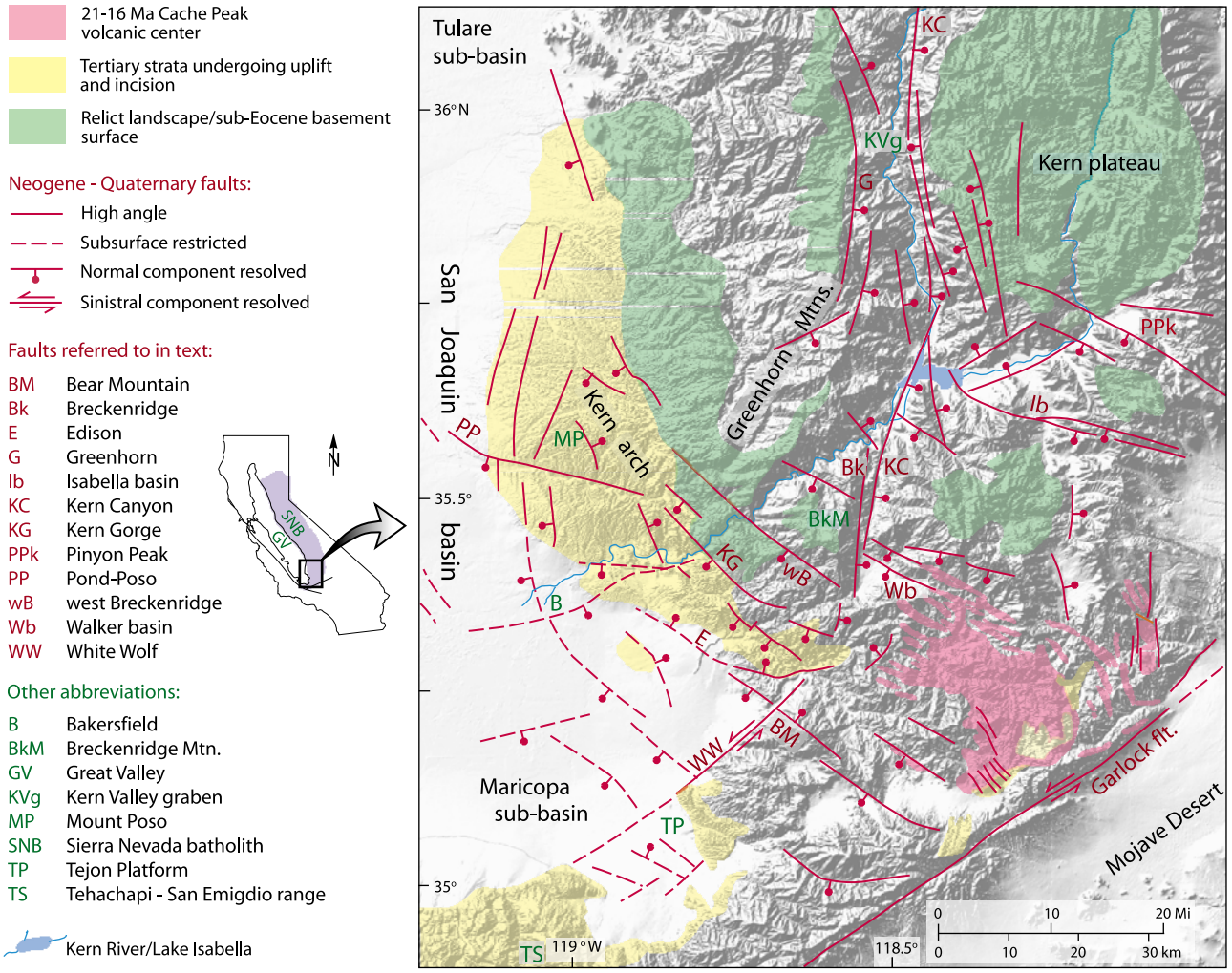

Figure 1. Digital elevation model of the southern Sierra Nevada showing tectonic, geographic, and geomorphic features referred to in text. Southern reaches of Sierra Nevada regional relict landscape surface modified after *Clark et al.* [2005]. Sources for structural data are given in Text S1.

[4] We apply the apatite He method to the study of the geomorphology and structure of the southern Sierra Nevada between latitudes 35.2°N and 36°N (Figure 1). Bedrock exposures in this region are composed of ~90% Cretaceous batholithic rock and ~10% metamorphic pendant rock, with relatively sparse Cenozoic deposits and Miocene volcanic/hypabyssal rocks [*Saleeby et al.*, 2008]. The geomorphology of this region reflects a pronounced transition from a vast region to the north characterized by nonequilibrium fluvial modification of a relict low relief landscape surface that is little affected by internal deformation [*Clark et al.*, 2005], to a more complex landscape affected by numerous late Cenozoic faults. By the use of the geomorphic expression of the relict landscape surface and the apatite He thermochronometric tagging of the surface, as well as underlying paleoisothermal surfaces, we reconstruct structural relief and tilt patterns of the batholithic basement imposed regionally and locally by late Cenozoic faulting. This analysis is further constrained by structural and stratigraphic relations in the adjacent eastern San Joaquin basin that is cut by the same fault system.

2. Analytical Methods

[5] We analyzed apatites from granodiorites and tonalities that yield U/Pb zircon (crystallization) ages in the 102–87 Ma range [*Saleeby et al.*, 2008]. Field sampling strategy was based on establishing a series of (near) vertical profiles as well as equal elevation transects within the physical limitations of the environment. Such limitations included areas of extreme relief or dense vegetation, evidence of past wild fires, and accessibility constraints. A number of these profiles and traverses focused on known or suspected faults based on geomorphic and structural relations. Out of 72 sample sites 63 yielded usable apatite separates (Figure 2). All the useable samples yielded numerous euhedral apatite grains (~70–200 μm prism cross section) for which the results of replicate analyses are summarized in Table 1. The

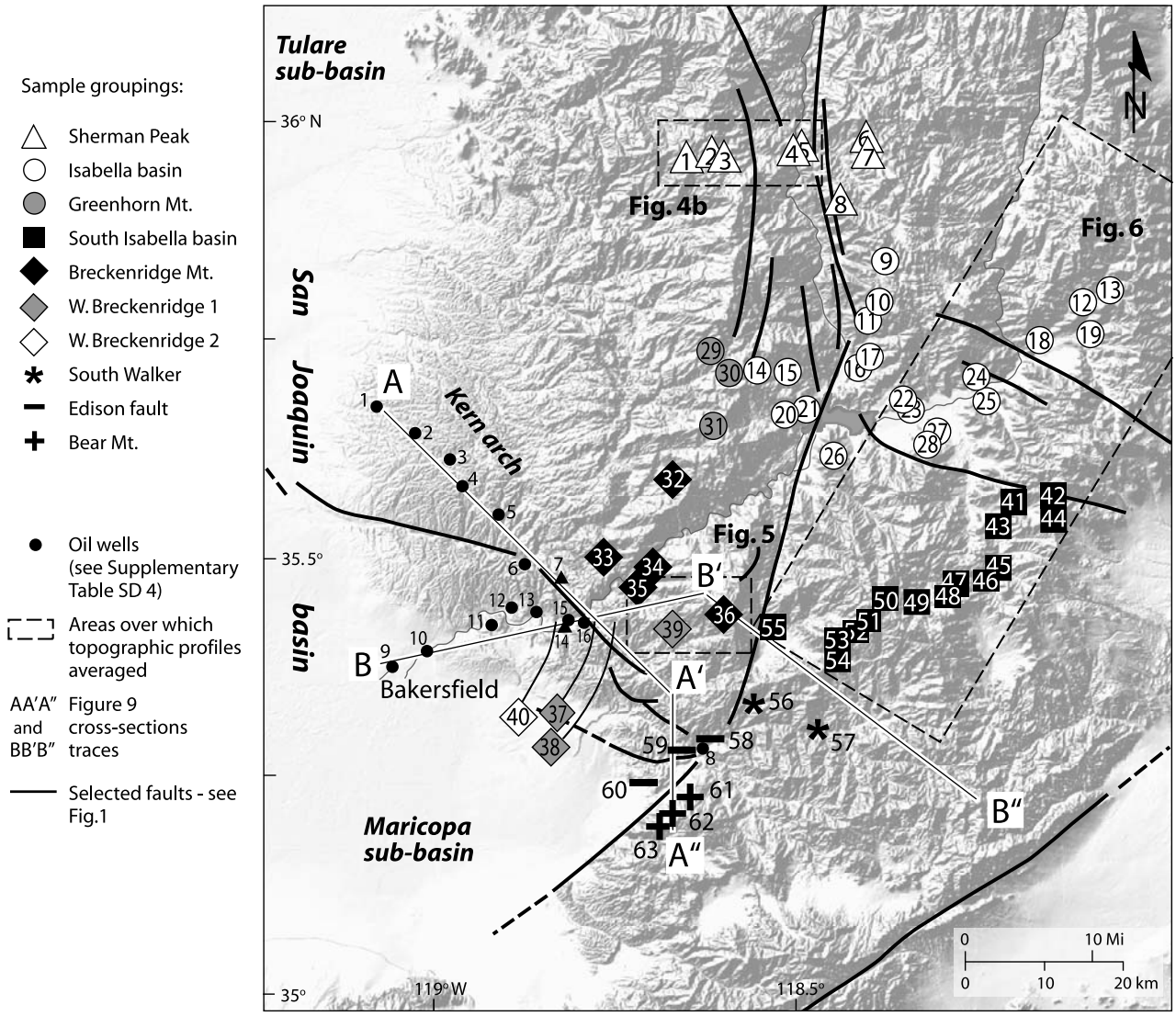

Figure 2. Apatite (U-Th)/He sample locations, and oil wells used for subsurface analysis plotted on a digital elevation model. Dashed boxes represent areas over which topographic profiles have been averaged on Figures 4b, 5, and 6. Symbols represent groupings of samples for structural and geomorphic analysis. Traces of Figure 9 cross sections shown as AA′A″ and BB′B″.

analytical techniques, as well as the tabulation of all of the analytical data are in Text S1.[1]

3. Geologic Setting

[6] The Sierra Nevada constitutes part of a semirigid crustal block that along with the coupled Great Valley has been termed the Sierra Nevada microplate [*Argus and Gordon*, 1991]. The dimensions of this "microplate" are ~600 km in N–S by ~250 km in E–W directions. It is bounded on the west by the San Andreas transpressive plate juncture and to the east by the eastern Sierra escarpment system. To the south, adjacent to the study area, it is bounded by the Garlock fault. Much of the Sierra Nevada may be characterized as a WSW tilted fault block whose tilting and related basement exhumation are balanced by a linear zone of subsidence and sedimentation in the Great Valley [*Unruh*, 1991]. This pattern breaks down in the southern Sierra region where the basement is extensively faulted and the western margin of the range is in part defined by a steep escarpment system. Likewise, the regional tilt and linear depositional trough pattern break

[1]Auxiliary material data sets are available at ftp://ftp.agu.org/apend/tc/2008tc002340. Other auxiliary material files are in the HTML.

Table 1. Mean Apatite (U-Th)/He Ages and Field Locations[a]

Sample	Location	UTM 11 Easting (m)	UTM 11 Northing (m)	Elevation (m)	Mean Age (Ma)	Error (Ma)	Number of Replicates
1	Sherman Peak	355276	3981293	1890	71.3	1.0	4
2	Sherman Peak	358464	3982266	1879	63.8	1.7	10
3	Sherman Peak	359875	3981996	1515	63.3	1.9	11
4	Sherman Peak	369102	3982400	1515	63.3	1.2	10
5	Sherman Peak	369942	3983109	1879	63.8	1.3	14
6	Sherman Peak	377174	3982623	3012	69.9	7.0	1
7	Sherman Peak	377166	3982264	2861	73.8	6.7	2
8	Sherman Peak	373324	3975470	2242	67.5	2.1	6
9[b]	Isabella basin	378160	3967682	2594	72.8	7.6	2
10	Isabella basin	377533	3962368	2245	60.9	2.3	16
11[b]	Isabella basin	375583	3960319	1879	60.0	0.9	4
12	Isabella basin	401910	3959844	1515	62.8	4.5	13
13	Isabella basin	405078	3961053	2200	62.4	2.4	10
14	Isabella basin	361348	3954681	1515	56.8	5.7	1
15[b]	Isabella basin	364450	3954054	1152	50.9	2.2	4
16[b]	Isabella basin	375232	3954587	1152	52.6	0.4	4
17[b]	Isabella basin	375523	3955154	1515	54.8	1.7	3
18[b]	Isabella basin	396674	3955575	1152	49.3	2.0	3
19[b]	Isabella basin	402279	3955470	1155	49.5	1.1	2
20[b]	Isabella basin	365275	3948166	1150	46.7	2.4	4
21	Isabella basin	367476	3948830	788	45.3	1.5	4
22[b]	Isabella basin	379055	3949184	1147	46.8	2.0	3
23	Isabella basin	379868	3948285	794	46.3	0.8	21
24	Isabella basin	388243	3951314	1152	45.9	4.6	1
25[b]	Isabella basin	388900	3948502	1152	52.4	2.8	9
26	Isabella basin	369848	3942935	1648	60.3	3.9	3
27[b]	Isabella basin	383034	3944675	1152	52.9	1.5	4
28	Isabella basin	382276	3943380	1515	54.7	1.8	4
29	Greenhorn Mountains	356667	3957198	1509	45.0	1.1	2
30	Greenhorn Mountains	359027	3955187	1891	52.1	0.5	2
31	Greenhorn Mountains	356307	3947827	1885	57.0	0.5	14
32	Breckenridge Mountain	350708	3940938	1506	60.9	0.9	8
33	Breckenridge Mountain	342057	3931758	924	69.6	3.9	4
34	Breckenridge Mountain	346719	3929695	530	61.7	0.9	2
35	Breckenridge Mountain	344820	3927344	461	64.4	2.0	8
36	Breckenridge Mountain	355718	3924033	2248	65.0	1.6	8
37	W Breckenridge 1	339390	3924149	939	72.7	4.3	4
38	W Breckenridge 1	340040	3924297	279	72.0	1.7	4
39	W Breckenridge 1	349822	3923195	1048	68.4	1.1	4
40	W Breckenridge 2	335263	3925305	342	67.9	0.8	4
41	South Isabella basin	392601	3935901	1197	61.6	1.7	8
42	South Isabella basin	396405	3935568	1536	52.0	1.7	8
43	South Isabella basin	391015	3932556	1164	49.7	0.7	8
44	South Isabella basin	396529	3933080	1891	59.5	2.0	8
45	South Isabella basin	389557	3926636	1258	48.2	1.5	8
46	South Isabella basin	388629	3925972	1515	56.0	1.9	8
47	South Isabella basin	384771	3924533	1900	53.2	2.3	8
48	South Isabella basin	384001	3924389	2000	53.5	1.6	8
49	South Isabella basin	380280	3923122	1879	53.2	2.4	7
50	South Isabella basin	376370	3924106	2242	53.8	1.2	9
51	South Isabella basin	374256	3923163	2497	58.9	1.4	8
52	South Isabella basin	373067	3921963	2242	54.6	1.5	8
53	South Isabella basin	371086	3920961	1874	49.8	1.4	8
54	South Isabella basin	371523	3918853	1515	42.9	1.2	8
55	South Isabella basin	362294	3922238	1151	46.1	1.1	13
56	South Walker	358748	3912874	1149	25.7	4.5	8
57	South Walker	368601	3907840	788	14.8	0.3	8
58	Edison fault	355930	3907909	456	49.3	3.0	9
59	Edison fault	350489	3906500	425	41.0	3.8	5
60	Edison fault	348337	3903629	561	16.8	0.4	5
61	Bear Mountain	351446	3901014	1158	28.7	1.0	8

Table 1. (continued)

Sample	Location	UTM 11 Easting (m)	UTM 11 Northing (m)	Elevation (m)	Mean Age (Ma)	Error (Ma)	Number of Replicates
62	Bear Mountain	350384	3899048	1485	58.0	0.8	8
63	Bear Mountain	349061	3897426	1818	53.5	1.8	7

[a]The error (1σ) is taken as the standard deviation divided by the square root of the number of replicates minus one, except samples with only one replicate for which a conservative 1σ error corresponding with 10% of the obtained age.
[b]Data from *Clark et al.* [2005]; see text for details. See Figure 2 for location. Details of replicate analyses are available in Data Set S1.

down in the southern Great Valley, which is also extensively faulted.

[7] The geomorphology of the Sierra Nevada has been studied recently by field and high-resolution digital elevation analysis, low-temperature thermochronometry, and cosmogenic dating of cave sediments [*House et al.*, 1997, 1998, 2001; *Stock et al.*, 2004; *Clark et al.*, 2005; *Cecil et al.*, 2006]. These studies show that following the Late Cretaceous termination of large-volume magmatism, the Sierra Nevada region underwent slow erosional denudation through the early Cenozoic to form a low-relief landscape with widely spaced, west draining river canyons. The southern reaches of this relict landscape surface are shown on Figure 1. A detailed description of the surface for the Kern plateau and Greenhorn Mountains (Figure 1), and continuing through areas as far north of the study area as ~38°N is presented by *Clark et al.* [2005]. The surface as described by Clark et al. is well expressed along the west slopes of the Greenhorn Mountains and Breckenridge Mountain, and is further constrained by our mapping of it into continuity with the basal nonconformity of the eastern San Joaquin basin section as exposed along the Kern arch (Figure 1).

[8] During the Late Cretaceous–early Cenozoic the Sierra Nevada region constituted the southwest margin of a Cordilleran-wide orogenic plateau, from which the Sierra Nevada microplate was calved off during the late Cenozoic westward encroachment of Basin and Range extension to the area of the eastern Sierra escarpment [cf. *Saleeby et al.*, 2009]. The low-relief relict landscape surface began erosional rejuvenation by steep mainly west draining river incision patterns at post-20 Ma time [*Clark et al.*, 2005; *Clark and Farley*, 2007], presumably in response to microplate inception. A recent phase of accelerated river incision began at ca. 3 Ma, presumably in response to uplift driven by underlying mantle lithosphere foundering [*Saleeby and Foster*, 2004; *Zandt et al.*, 2004]. These incision events, in concert with the eastern range front faulting, give the Sierra Nevada its overall morphologic character of mainly west draining deep river gorges separated by broad low-relief interfluves. This pattern breaks down south of latitude 36°N where the Kern River forms major south draining branches that join in Isabella basin where the main trunk bends southwestward and continues as the lower Kern River gorge that drains into the San Joaquin basin (Figure 1). Isabella basin is an anomalous geomorphic feature forming an alluviated intermontane basin that has resulted from the partial damming of Kern River sediments by Quaternary west-side-up motion on the Kern Canyon fault. Walker basin forms another anomalous depression partly as a result of west-side-up motion on the Breckenridge fault (Figure 1). Such fault controlled internal basins are absent in the Sierra Nevada north of latitude 35.7°N.

[9] The effects of late Cenozoic faulting are expressed throughout the study area. These faults are defined as the southern Sierra fault system, with two principal sets oriented ~N–S and NW, and a subordinate set NE (Figure 1). Fresh scarps and triangular faceted topographic fronts indicating Quaternary west-side-up normal motion are common along the Kern Canyon zone and continue southwards as the Breckenridge fault [*Ross*, 1986; *Nadin*, 2007; *Saleeby et al.*, 2009]. The Kern Gorge fault also forms a pronounced Quaternary northeast-side-up normal escarpment along the west margin of the range [*Gilbert*, 1928]. Quaternary normal faulting is densely distributed across a broad uplift immediately to the west of the range front forming a salient in the San Joaquin basin named the Kern (River) Arch [*Edwards*, 1943], or Bakersfield Arch of *Hoots et al.* [1954]. The southern margin of the San Joaquin basin (Maricopa subbasin) is bounded in part by active basement uplift and sinistral motion along the White Wolf fault, and further west by active north ramping thrusts that root southwards beneath the San Emigdio-Tehachapi fold-thrust belt [*Nilsen et al.*, 1973; *Davis and Lagoe*, 1988; *Clinton et al.*, 2006].

[10] A distinct phase of early to middle Miocene growth faulting and associated volcanism is recorded in the subsurface of the Maricopa subbasin and Tejon Platform [*MacPherson*, 1978; *Hirst*, 1986; *Goodman and Malin*, 1992]. In parallel early to middle Miocene volcanism and associated faulting is recorded in the area of Walker basin and the adjacent Cache Peak volcanic center (Figure 1). Motion along the Walker basin fault zone was accompanied by the emplacement of closely spaced dikes sourced from the volcanic center. Figure 1 shows the distribution of some of the larger dikes. There are many more dikes and small plugs than shown. A number of dikes lie within the eastern extension of the Walker basin fault zone, and some possess shear fabrics that are compatible with normal sense shear along the fault zone. Growth faulting within the Cache Peak volcanic sequence along NW striking normal faults that parallel the Walker basin zone further indicate that the principal phase of movement along NW striking normal faults of the Walker basin area was coincident with construction of the Cache Peak center. K/Ar and Ar/Ar ages of the volcanic center and remnants of its distal apron are between 16.5 and 21.4 Ma [*Evernden et al.*, 1964; *Bartow and McDougall*, 1984; *Coles et al.*, 1997]. These are

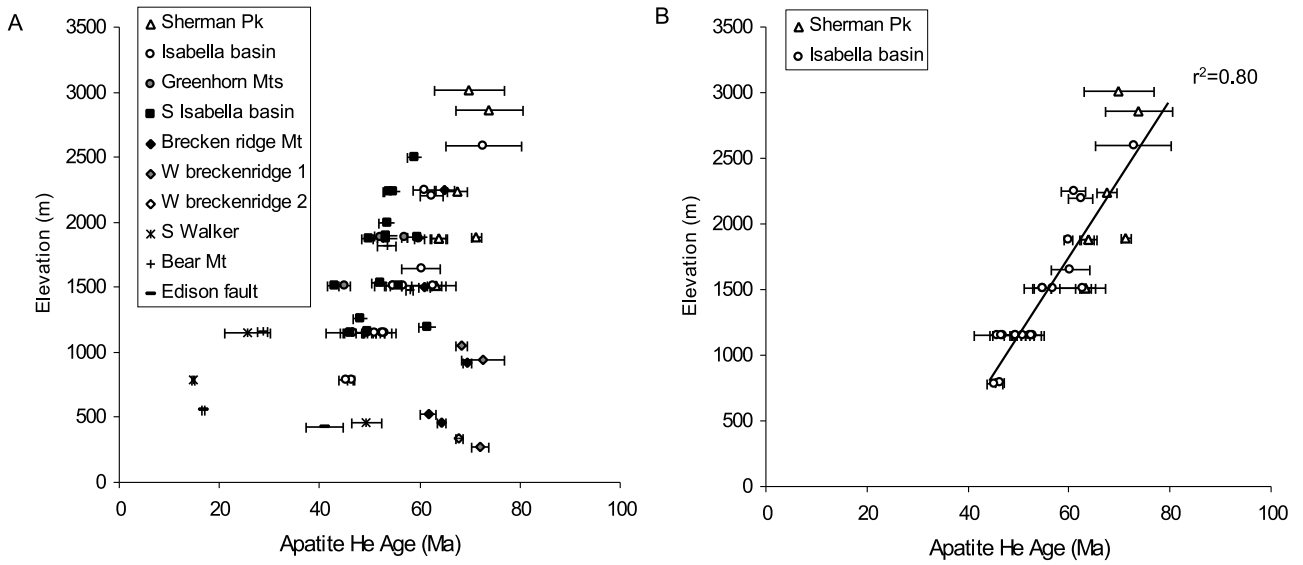

Figure 3. Age elevation relationship for southern Sierra Nevada apatite He samples. (a) all data and (b) Sherman Peak (samples 1 to 8) and Isabella basin (samples 9 to 28).

interpreted as an age constraint on the principal phase of motion on the Walker basin zone.

[11] Structural, geochronologic, and high temperature thermochronometric data indicate that many of the principal faults of the southern Sierra system originated in the Late Cretaceous, and have thus been remobilized in late Cenozoic time [*Wood and Saleeby*, 1997; *Nadin and Saleeby*, 2008]. The fault system is unique to the southern Sierra Nevada and adjacent San Joaquin basin, and not present elsewhere in the microplate. This stems from the fact that the tectonics responsible for the initial Late Cretaceous penetrative fracturing and faulting of the region were unique to the southern Sierra region, and did not affect the greater Sierra Nevada and Great Valley to the north [*Saleeby*, 2003]. The late Cenozoic phase of faulting is also lacking to the north, in the face of very different regional tectonic regimes having operated in Late Cretaceous versus late Cenozoic time. This suggests that structural inheritance played an essential role in the late Cenozoic phase of faulting in the region.

4. General Apatite (U-Th)/He Age Distribution in the Southern Sierra Nevada

[12] The field locations of the samples studied are shown on Figure 2. The apatite He ages range between 15 Ma and 74 Ma with the youngest located in structural depressions in the south, and the oldest in higher structural positions in the Sherman Peak area and along the west slope of Breckenridge Mountain. All of the apatite He ages plotted together on an age-elevation diagram yield a positive correlation for higher elevation samples and considerable scatter for lower elevation samples (Figure 3a). Samples from the Isabella basin to the Sherman Peak area define an age–elevation relationship ($r^2 \sim 0.80$) with an apparent exhumation rate of 0.06 mm/yr (Figure 3b). This rate is comparable to rates determined throughout the greater Sierra Nevada to the north [*House et al.*, 2001; *Clark et al.*, 2005; *Cecil et al.*, 2006] and is typical for much of Cenozoic time across the relict landscape surface. The older ages of the Sherman Peak area and from the west slope of Breckenridge Mountain are consistent with geomorphic observations of those areas being characterized by deeply weathered flat topped interfluves suggesting that the interfluve tops are remnants of the relict landscape surface. Other parts of the study area do not yield apatite He ages with such a simple relationship to the regional geomorphology.

[13] West of Isabella basin, in the Greenhorn Mountains, the ages are slightly younger than those of Isabella basin. South of Isabella basin age distribution is more complex and age–elevation relationships cannot be resolved. Between Isabella basin and Walker basin, N–S constant elevation profiles are characterized by a progressive southward decrease of ages (Figure 4a). Further south, between Walker basin and Bear Mountain, the samples yield ages with a wide spread between 14.8 Ma and 56.0 Ma. Some of these samples have poor reproducibility and the two with good reproducibility have anomalously young ages (14.8 Ma and 16.8 Ma). We interpret these samples to have been disturbed beneath a section of Neogene volcanogenic strata. In addition to this disturbance complication, samples that yield apatite He ages that cannot be readily related to the regional landscape patterns are interpreted below in the context of late Cenozoic faulting.

5. Interpretation of the Apatite He Age Distribution Patterns

[14] Apatite He ages are published for the Sierra Nevada in regions north of latitude 36°N [*House et al.*, 1997, 1998, 2001; *Clark et al.*, 2005; *Cecil et al.*, 2006]. These data in general form coherent arrays that can be related to landscape

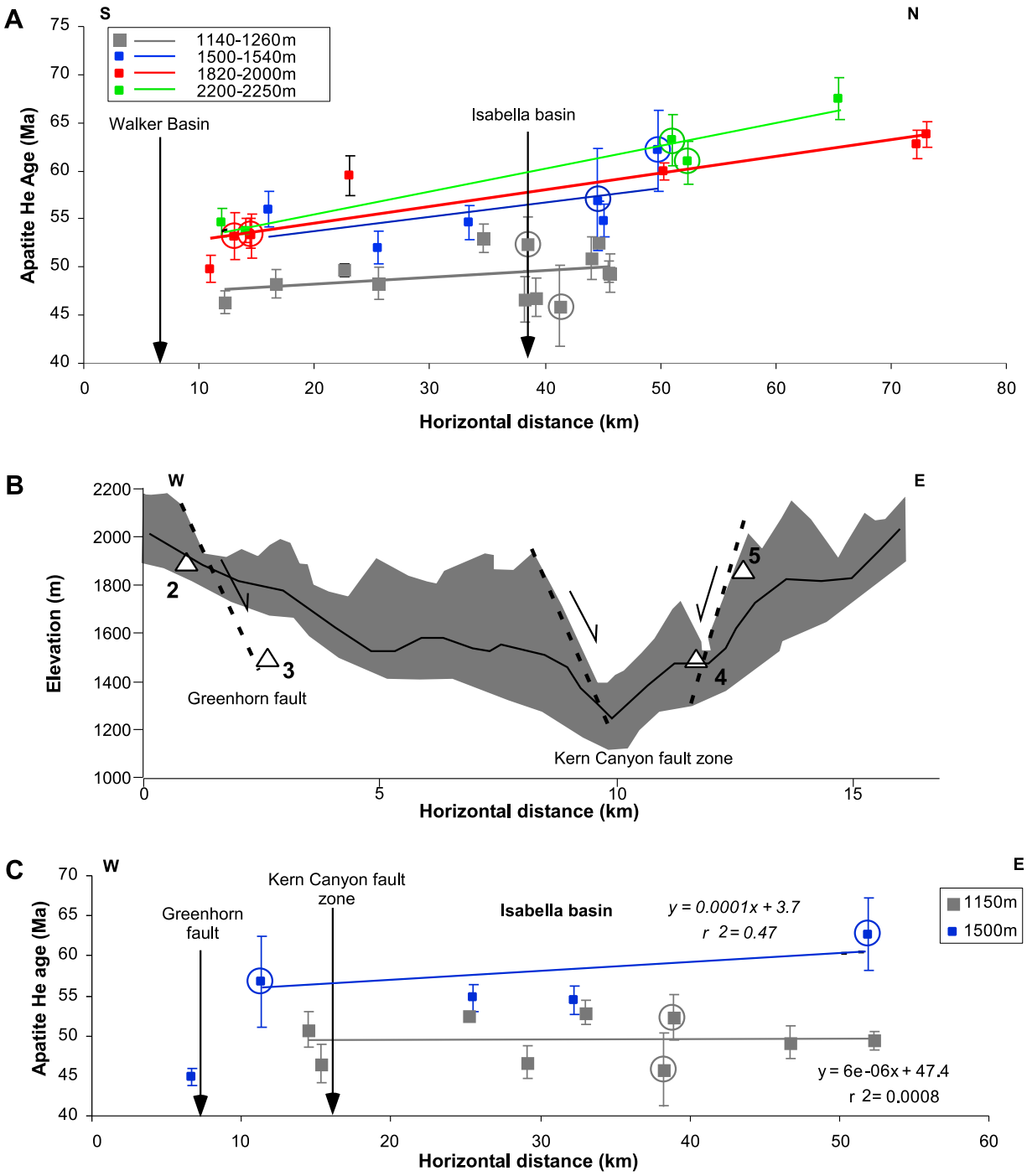

Figure 4. (a) Apatite He age versus distance along a north–south traverse across Isabella basin for samples with similar elevation (1140–1260 m: samples 15, 16, 18–20, 22, 24, 25, 27, 41, 43, 45 and 55; 1500–1540 m: samples 12, 14, 17, 28, 42 and 46; 1820–2000 m: samples 2, 5, 11, 44, 47–49 and 53; 2200–2250 m: samples 8, 10, 13, 50 and 52). Samples inside the Kern valley graben have not been used. (b) Relationship between topography and elevation for samples with the same apatite He age (62 to 63 Ma) in the Sherman peak area. See Figure 2 for area over which 18 parallel profiles from SRTM digital elevation have been averaged. Shaded area represents range of profiles averaged and solid line the average. (c) Apatite He age versus distance along an east–west traverse across Isabella basin for samples with similar elevation (~1150 m: samples: 15, 16, 18–20, 22, 24, 25 and 27; ~1500 m: samples 12, 14, 17, 28 and 29). In all plots, circled samples have either a high replicate age spread (>10% of the mean age) or only one replicate.

development controlled by regional tectonic forcing. This contrasts markedly with the age distribution of the study area. This suggests that in the study area either the isotherm corresponding to the closure temperature of He in apatite (~75°C) had a more complex geometry than in regions to the north, or that tectonically induced differential vertical motion has occurred between the samples. In the following sections we will discuss the relationships between age distribution, geomorphology and structural observations, and discuss whether the isotherm shape is a consequence of geomorphology, or if the geomorphic and structural evidence for faulting explains the age patterns.

5.1. Resolution of Normal Faults Within Batholithic Rocks Based on Apatite He Age Offsets

[15] The Kern River Valley area north of Isabella basin is marked by numerous ~N–S trending lineaments and discontinuous fault scarps that run parallel to the valley (Figure 1) [*Nadin*, 2007; *Saleeby et al.*, 2009]. Structural and geomorphic relations of the scarps suggest high-angle normal motions. Some of the scarps and lineaments clearly follow the Late Cretaceous ductile/brittle damage zone of the Kern Canyon fault system, lying along lithologic contacts and/or discontinuities in transverse strain gradients. Others occur within otherwise homogeneous batholithic units outside this damage zone, and are more cryptic to field resolution. Apatite He age patterns across some of the prominent lineaments clearly show the effects of vertical components of faulting. In the Sherman Peak area a plot of the elevations of samples with comparable ages (62–63 Ma) versus easting correlates with local topography (Figure 4b). The geomorphology in this area is characterized by an open valley that is ~12 km wide and ~500 m deep, which is incised in the middle by the Kern River. The morphology of the valley as well as the abrupt change in the elevations of the 62–63 Ma age range samples rule out topographic effects as the cause of the age distribution [i.e., *House et al.*, 2001]. The age distribution is interpreted to result from faulting. Considering the geomorphology and the spatial relations of the age-elevation plot, the open valley is interpreted as a ~N–S trending graben. We term this feature the Kern Valley graben. Late Quaternary west-side-up normal scarps of the Kern Canyon zone lie within the graben. Based on the apatite He ages the minimum vertical offset along the east wall of the graben in the Sherman Peak area is ~400 m, which is similar to the offset suggested by the local topography. The west wall of the graben has undergone considerable erosion in this area, but in general corresponds to a 200–400 m step in topography. We name the west bounding structure the Greenhorn fault, after the Greenhorn Mountains whose elevated state arises from footwall uplift (Figure 1). Two equal elevation samples collected along an east–west profile of the footwall (1 and 2) yield significantly different ages. The ages increase westward from 63.8 Ma (2) to 71.3 Ma (1). Such age variation is compatible with a westward tilting related to the Greenhorn fault, and possibly the young scarps of the Kern Canyon zone as well.

[16] For the analysis of the western part of Isabella basin we plot the ages of samples collected at comparable elevations (~1100 m and ~1500 m) versus easting (Figure 4c). Most of the samples do not show significant age differences, except for the westernmost sample that is anomalously young for its elevation and lies in the footwall of the Greenhorn fault, which in this location exhibits an ~N–S oriented ~500 m high topographic front. Based on the He ages and assuming an apparent exhumation rate of 0.06 mm/yr, the Greenhorn fault in this area would have a minimum vertical offset of 600 m. The orientation and sense of displacement on the Greenhorn fault are consistent with a series of fresh scarps that are dispersed along the Kern Canyon–Breckenridge zone [*Ross*, 1986; *Nadin*, 2007; *Saleeby et al.*, 2009]. The advanced state of erosional modification of the structures bounding the Kern Valley graben, in conjunction with the relatively fresh discontinuous scarps within the graben suggests a protracted history of normal faulting across the graben. Active faulting along the east margin of the graben is expressed by the M~2–4 Durrwood Meadows seismicity belt [*Jones and Dollar*, 1986].

5.2. Normal Faulting in the Breckenridge Mountain Area

[17] Geomorphic patterns as well as structure mapping indicate that the Breckenridge Mountain area is cut by normal faults. Several samples have been collected from this area, including its western slopes down across the range front (Figures 1 and 2). Their apatite He ages further define the principal faults as well as tilt patterns. Our analysis recognizes four structural domains in this area from east to west: (1) the hanging wall of the Breckenridge fault, which in part defines Walker basin. (2) The Breckenridge Mountain area that is capped in its summit area by the relict landscape surface [*Clark et al.*, 2005]. (3) The west Breckenridge Mountain slope, which constitutes a southwest-side-down fault block, relative to the Breckenridge summit area. (4) The hanging wall of the Kern Gorge fault, which consists primarily of Cenozoic strata, but with local basement exposures proximal to the fault. The Kern Gorge fault and the Breckenridge fault are recognized as young, potentially active normal faults [*Gilbert*, 1928; *Ross*, 1986; *Nadin*, 2007; *Saleeby et al.*, 2009]. Our geomorphic analysis and structure mapping resolves an additional important fault that forms a west facing ~1300 m high topographic front that divides the summit area of Breckenridge Mountain from its western slopes. This structure consists of a northeast-side-up normal fault zone that we name the west Breckenridge fault. Unlike the Kern Gorge and Breckenridge faults, youthful scarps have not been recognized along the west Breckenridge fault, and its topographic front has undergone substantial erosion. Nevertheless, the position, orientation and sense of motion on this fault suggest that it is closely aligned with the Kern Gorge fault. The Kern Gorge and west Breckenridge faults together form the southwest face, and the Breckenridge fault forms the east face of a northward widening basement uplift (Figure 1). The northward continuation of the east face of the uplift is the footwall of the Greenhorn fault as well as young scarps of the Kern Canyon zone (Figure 1). We define this wedge-shaped uplift as the Breckenridge-Greenhorn horst.

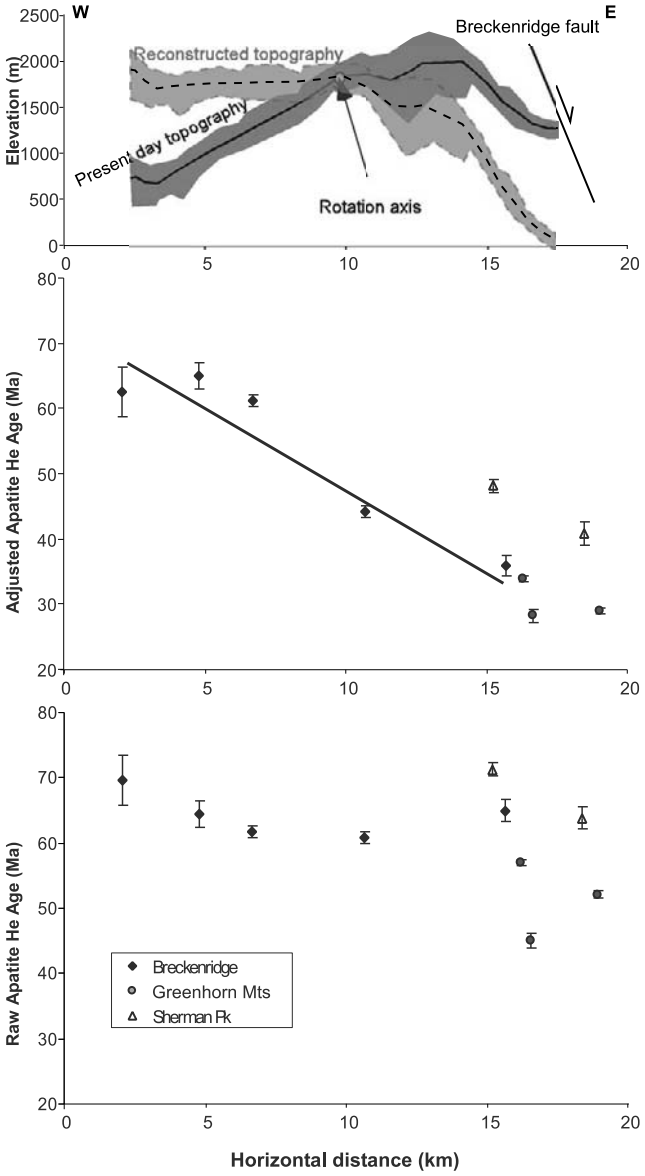

Figure 5. (top) Topographic profile of Breckenridge Mountain area in relation to Breckenridge fault and distribution of adjusted apatite He ages versus easting for Breckenridge area (samples 32 to 40), Greenhorn Mountains (samples 29 to 30), and Sherman Peak samples 1 and 2. (middle) The ages have been adjusted to a constant elevation of 500 m using an apparent exhumation rate of 0.06 mm/yr. Age adjustment data in Table S2. (bottom) Raw ages also shown for comparison to adjusted ages. Averaging of topography same methodology as for Figure 4. The reconstructed topography (light gray area and associated dashed average line) obtained by tilting the present-day topography 9° at 1:1 scale. The rotation axis was chosen at sample 36, located on the relict landscape surface of Breckenridge Mountain and yielding the same age as the Isabella basin samples at comparable elevations.

[18] Three samples (33, 34 and 35) collected along a vertical profile provided by the lower Kern River gorge through the Breckenridge-Greenhorn horst give an apparent exhumation rate of 0.06 mm/yr, identical with those obtained further north and east. However, if all the samples from this area are plotted together no clear age elevation relationship is resolved. In order to better analyze the distribution of the ages in this area and their possible relationship with west-side-up normal faulting on the Breckenridge fault we adjusted the footwall ages to a common elevation of 500 m based on the 0.06 mm/yr apparent exhumation rate (age adjustment data in Table S2). The plot of the adjusted ages versus easting is characterized by an eastward decrease in age of ~35 Myr over a horizontal distance of ~13.5 km (Figure 5). This pattern is compatible with a west tilt associated with west-side-up normal motion along the Breckenridge fault. To this sample suite we added the three southern samples from the Greenhorn Mountains suite (29, 30 and 31), located along the northern continuation of the horst. These samples extend the observed pattern and suggest that the entire Breckenridge-Greenhorn horst was tilted uniformly. Moreover, if we also plot the two samples from the Sherman Peak suite located west of Greenhorn fault (1 and 2), the same pattern emerges, but with a shift toward older ages (Figure 5). This suggests that the Greenhorn fault is kinematically linked to the Breckenridge fault, but probably with a lower vertical offset. Field observations suggest that the Breckenridge fault continues as west-side-up scarps that lie in continuity with those of the Kern Canyon zone within the Kern Valley graben. For the Breckenridge-Greenhorn horst samples, the 35 Myr age difference corresponds to a minimum vertical offset of ~2.1 km along the Breckenridge fault, and a tilt of ~9° to the west. Such a tilt is similar to the west slope of Breckenridge Mountain, thus by restoration of the estimated 9° tilt the modern topographic surface across the top of the horst rotates to near horizontal (Figure 5). The 9° west tilt is also similar with the topographic slope west of the Greenhorn fault which suggest that this area is the northward continuation of the tilted surface previously recognized on Breckenridge Mountain. We suggest that west-side-up motion of the Kern Canyon scarps and Greenhorn fault sum to a value comparable to that of the Breckenridge fault yielding a regionally consistent west-side-up displacement and west tilt.

[19] All of the apatite He ages obtained along the west slope of Breckenridge Mountain are relatively old, and do not change appreciably with elevation (Figure 3a). This domain is characterized by deeply weathered flat-topped interfluves, which along with relatively old apatite He ages suggests that the interfluve surfaces are erosional remnants of the regional relict landscape surface. The relatively old ages that are comparable with those of the Breckenridge Mountain summit area facilitates the estimation of vertical throw across the west Breckenridge fault by matching up the relict landscape surface across the fault. Inasmuch as the relict surface is preserved in the Breckenridge Mountain summit area, as well as along the hanging wall interfluve surfaces, the vertical throw should be approximated by the elevation difference across the topographic front resulting

from the fault. Based on digital elevation data we estimate that front to be ~1300 m high. This vertical throw estimate can be further tested by comparing the relative elevations of samples taken from footwall and hanging wall domains on what were interpreted, based on geomorphology, to be erosional remnants of the relict landscape surfaces (36, 2348 m, 65.0 ± 1.6 Ma, and 39, 1048 m, 68.43 ± 1.9 Ma). The relatively old and nearly coincident ages of these two samples confirms our interpretation of the sample sites lying on, or very near the relict landscape surface. The vertical offset of the relict surface based on this analysis is ~1300 m. We thus approximate the vertical throw on the west Breckenridge fault to be 1300 m.

[20] The relict landscape surface is well expressed along interfluve tops from the west Breckenridge fault westward to the steep topographic front of the Kern Gorge fault (Figure 1). To the north this surface maps out in continuity with the basal Eocene nonconformity of the San Joaquin basin. Samples 37 and 38 were taken as a vertical transect through the footwall in the Kern gorge fault adjacent to the range front. Their relatively old ages are the same, within uncertainty, and do not define an age-elevation relationship. The samples from this area record an older phase of rapid exhumation that is not recorded in the other samples of the study area, and that is characteristic of the southernmost Sierra Nevada and Tehachapi range [*Saleeby et al.*, 2007]. Sample 40 was taken from the hanging wall of the Kern Gorge fault, adjacent to the nonconformity surface. Its age is very close to those of samples 37 and 38, and thus it only constrains the magnitude of Kern Gorge faulting to a value that is consistent with the relict landscape surface locally mapping into continuity with the Eocene nonconformity. The topographic relief on the range front in this area is ~600–700 m, which is taken as the structural relief, or throw on the fault, given the offset sub-Eocene surface.

5.3. Evidence of Normal Faulting and Tilting Between Isabella Basin and Walker Basin

[21] North–south constant elevation profiles between Isabella basin and Walker basin are characterized by a progressive southward decrease in apatite He ages (Figure 4a). Such a relationship indicates that either the closure temperature isotherm was gently dipping northward, or it was horizontal when the samples crossed it and has been subsequently tilted. Geomorphic relations and normal fault geometry suggest the latter. The relict landscape surface can be recognized between Isabella basin and Walker basin (Figure 1), and can be used to constrain late Cenozoic deformation of the area. In contrast to the gentle regional south slope to the surface across the Kern plateau, the surface between Isabella and Walker basins slopes northward more steeply. This relationship can be used in conjunction with the apatite He age distribution and mapped faults to constrain the amount of fault offset and related tilting. If the apatite He age distribution is only controlled by the isotherm morphology, or post cooling tilt, then for a given age the sample sites should define a plane in longitude-latitude-altitude space, assuming the isotherms and/or deformation geometry are planar. Moreover, if the tilting occurs after all the samples reached their closure temperature, then all such planes calculated for each age should be parallel. We use a procedure in which we pair samples with the same apatite He age within 5 Myr and separated by a least 5 km, and then calculate the trend and plunge of the line containing the two samples (Text S1 and Figure S1). We derive a statistical best fit solution for the sample groups, which yields 3.3°NE tilt about a horizontal axis of N40°W.

[22] Geological relations further suggest that the southward decrease in the apatite He ages has resulted from a tilted paleoisotherm. Walker basin is bounded on the west by the Breckenridge fault, and on the northeast by the Walker basin fault zone (Figure 1). The Walker basin fault zone has a southwest facing topographic front reaching 1000–1500 m above the basin floor with a mean slope of ~11° (Figure 6a). The back of the topographic front is characterized by a ~20 km long, NE sloping surface with a mean slope of ~4° that intersects the southern edge of the Isabella basin. Isabella basin morphology is more complex. It is an ~E–W trending basin developed east of the Kern Canyon fault, and it is crossed by a system of NW striking northeast-side-up normal faults and distributed brittle shear zones, and subsidiary NE striking southeast-side-up normal faults (Figure 1). The northern edge of Isabella basin is an ~1500 m high irregular topographic front with a mean slope of ~6°. This morphology would produce a significant deformation of the 75°C isotherm, i.e., deepest beneath the Isabella basin and shallowest beneath the southern margin of the Kern plateau. If similar topography existed during the exhumation of the studied samples, for a given elevation, samples located in the basin should be older than on the plateau, giving a negative age correlation with topography. However, if elevation-adjusted apatite He ages (for an exhumation rate of 0.06 mm/yr and a constant elevation of 1500 m; Table S3) are plotted versus distance along a N50°E trending trace (i.e., parallel to the tilting direction) a

Figure 6. (a) (top) Relationship between topography and adjusted apatite He ages for Walker basin to Isabella basin area. (U-Th)/He apatite ages are adjusted for a common elevation of 1500 m using an apparent exhumation rate of 0.06 mm/yr (samples used: 9–13, 16–19 and 22–55). Samples located outside of the zone considered for the topographic profile are in gray (9–11, 16, 17 and 26); samples inside the zone are in black. Age adjustment data are reported in Table S2. (middle) Raw ages also shown for comparison to adjusted ages. (bottom) All adjusted ages projected on a N50°E profile based on the ~N40°W tilt axis determined on Figure S1. Averaging of topography same methodology as for Figure 4, except 78 profiles averaged here (note that topographic profile in Figure 6a (bottom) was obtained on a smaller area than that covered by the samples that were projected onto Figures 6a (top) and 6a (middle)). Circled samples have either a high replicate age spread (>10% of the mean age) or only one replicate. (b) Restored topography between Isabella basin and Walker basin based on rotation axis related to normal faulting on Isabella basin fault. See text and Text S1 for explanation.

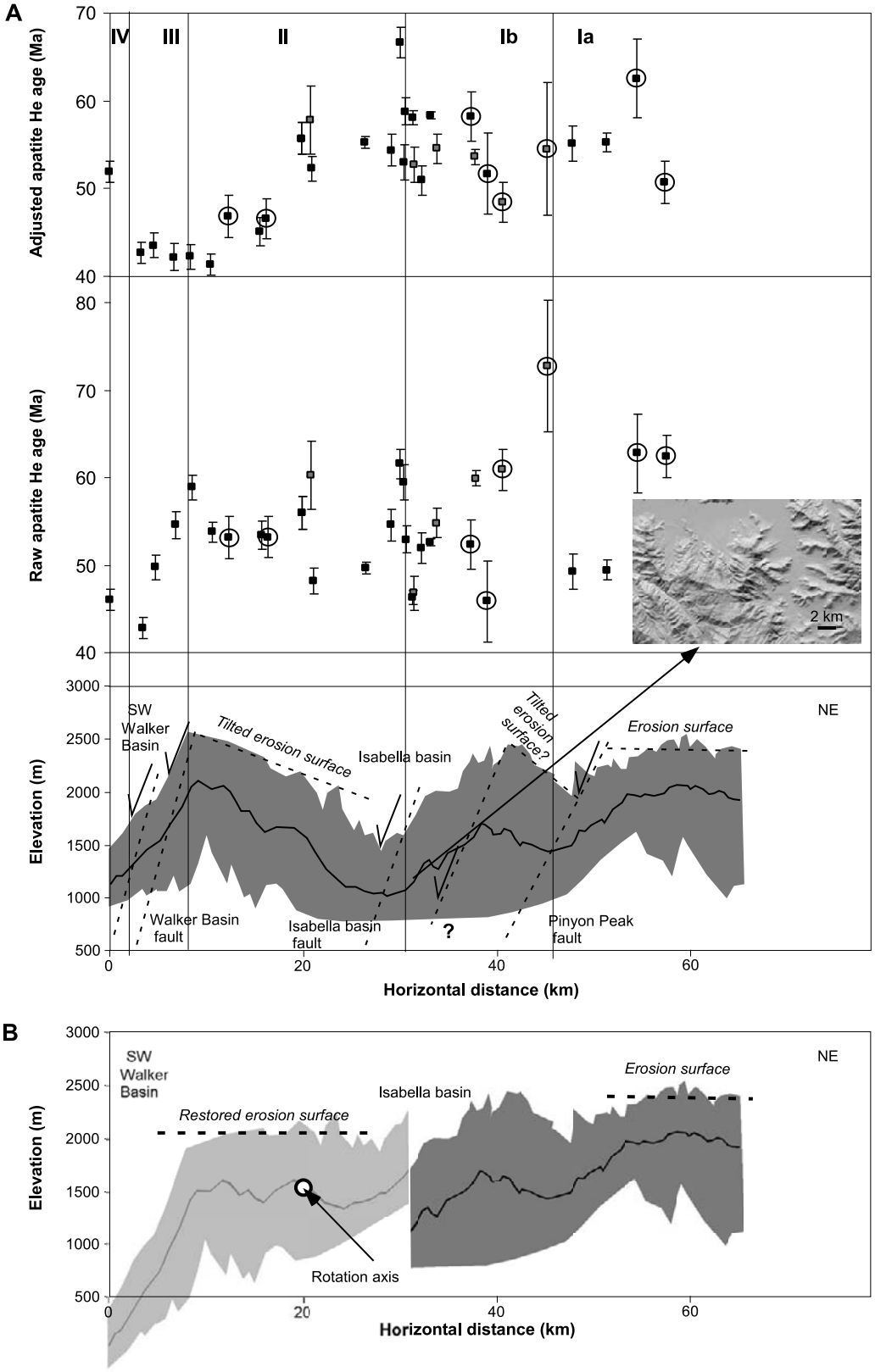
A
IV
III
II
Ib
Ia
Adjusted apatite He age (Ma)
Raw apatite He age (Ma)
2 km
SW
Walker
Basin
Tilted erosion surface
Isabella basin
Tilted erosion surface?
Erosion surface
NE
Elevation (m)
Walker Basin fault
Isabella basin fault
?
Pinyon Peak fault
Horizontal distance (km)
B
SW
Walker
Basin
Restored erosion surface
Isabella basin
Erosion surface
NE
Rotation axis
Elevation (m)
Horizontal distance (km)

Figure 6

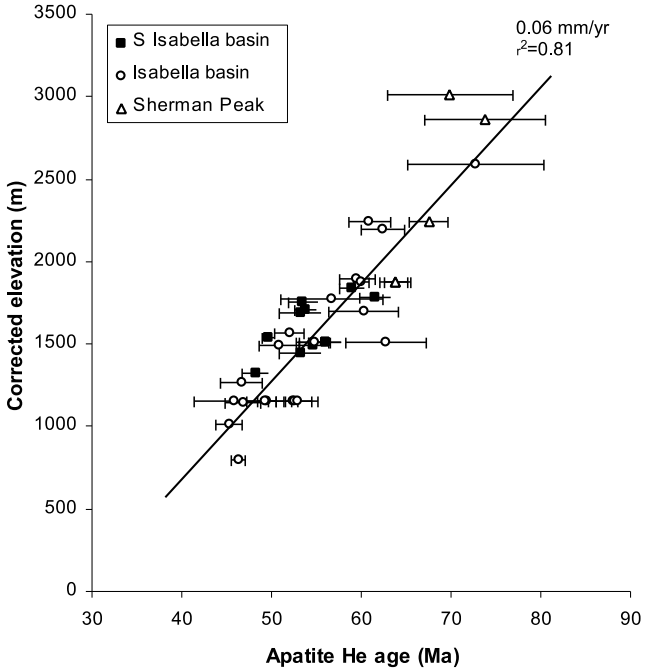

Figure 7. Apatite He age-elevation relationship for the Isabella basin, Sherman Peak and the South Isabella basin samples adjusted for tilting. Samples inside the Kern Valley graben (3 and 4) as well as sample 1 (tilted by the Greenhorn fault) have been excluded. Age adjustment data in Table S3.

northward decreasing age pattern that does not correlate with topography emerges (Figure 6a).

[23] From the topographic profile of Figure 6a it appears that the relict landscape surface is tilted northward in at least one, and possibly three panels. The main panel is bounded by the Walker basin and Isabella basin faults. Two additional panels are less clearly defined between the Isabella basin and Pinyon Peak faults. To test if the tilting of this surface is the same as that suggested by the apatite He ages, we restore the tilt observed in the topography by 3.3° about a N40°W axis. We have constrained the axis of rotation by searching for a sample within the principal tilted domain that has a similar apatite He age at a similar elevation to samples outside the tilted domain on the Kern plateau, and by passing the axis through the selected sample site. Sample 46 within the tilted domain, as compared to samples 12 and 17 of the Kern Plateau satisfy this constraint, within the uncertainties of the data (Figure 2 and Table 1). Rotation about this axis restores the tilted surface to a horizontal profile that projects northward into apparent continuity with the nonrotated relict landscape surface of the Kern plateau (Figure 6b). This suggests that the distribution of the apatite He ages and the morphology between Walker and Isabella basins are both controlled by the same tilting event. Such tilting is most readily explained by fault related rotations along a set of ~N40°W striking, SW dipping normal faults, most clearly defined for the Isabella basin and Pinyon Peak faults. The normal offset on the Isabella basin fault that corresponds to this tilt and its corresponding axis is ~700 m. A comparable amount of displacement is suggested for the Pinyon Peak fault (Figure 6a), but neither the geomorphic nor apatite He age data constrain this very well.

[24] The locations of the Walker basin, Isabella basin and Pinyon Peak faults, as determined in the field, can be confirmed by a plot showing the elevation-adjusted apatite He ages versus distance along the tilt direction (Figure 6a). In this plot, four zones can be distinguished: zones Ia and Ib include samples from the Isabella basin and northward scatter about a horizontal trend; zone II includes south of Isabella basin and up to the crest above Walker basin the ages progressively decrease to the SW; zone III includes south of the crest above Walker basin to the basin margin the ages remain constant; and zone IV includes the sample from the eroded scarp immediately above the basin floor is significantly older. The Ia-Ib transition corresponds to what we suspect is the transition from nontilted to tilted rocks across the Pinyon Peak fault, but precision limitations as well as uncertainty in identifying the tilted surface inhibit a more detailed interpretation. The transition from I to II corresponds to the Isabella basin normal fault zone. Southward across the transition from II to III, and III to IV at least two normal faults are observed to constitute the Walker basin fault zone. A third parallel fault, for which sample 55 sits in a footwall position, is indicated by geomorphic relations along the edge of the basin floor.

[25] The Isabella basin fault zone does not form a continuous topographic front. As the fault zone climbs southeastward out of the basin floor it coincides with a series of pronounced topographic lineaments, one of which forms a significant ~400 m high SW facing topographic front. The lineaments are well expressed on the Figure 6a DEM inset, extending ~N40°W across the inset diagonal. Further east this fault zone continues over a sharp saddle in the Sierra crest that is penetrated by closely spaced NW striking shear fractures within otherwise uniform batholithic rocks, and a series of springs. As the fault zone passes over the saddle area it forms an ~500 m SW facing topographic front. The topographic front arising from the Isabella basin fault has diffused northward within Isabella basin. This erosional diffusion appears to have been facilitated by the subsidiary NE striking normal faults, as well as a system of NW and NE striking fractures, and small offset shears and faults in batholithic rocks, all of which are concentrated in Isabella basin relative to adjacent areas. The present-day topographic front defining the north edge of Isabella basin is interpreted as the remnants of this erosional diffusion.

[26] To further test the validity of the tilted surface between Isabella and Walker basins as being the disrupted remnants of the relict landscape surface we now adjust the apatite He ages of the tilted block for the effects of tilting (Table S3), and plot these on an age-elevation graph along with apatite He ages from nontilted domains to the north on the Kern plateau (Figure 7). In Figure 7 we obtain a new age-elevation relationship with a strong positive correlation ($r^2 = 0.81$) and an apparent exhumation rate of ~0.06 mm/yr, the same as obtained for the Isabella basin and Sherman Peak areas alone. This confirms that the tilted surface is the

relict landscape surface, and the age–elevation relationship is valid for the entire region under consideration.

[27] Isabella basin is an important tectonic element of the southern Sierra Nevada. It approximates the horizontal hinge about which the southern Sierra Nevada batholith was rotated in the Late Cretaceous, ultimately leading to lower crust exhumation to the south [*Saleeby*, 2003; *Nadin and Saleeby*, 2008]. As a result Late Cretaceous transverse structures developed along the future trace of the basin [*Wood and Saleeby*, 1997], and these appear to have helped localize Neogene extensional faulting. To the north of the basin the Kern plateau constitutes relatively intact basement that lies in continuity with that of the high eastern Sierra. South of the plateau, and east of the Kern Canyon–Breckenridge zone, Sierran basement is broken by numerous extensional structures. Normal faults of Isabella basin thus form a breakaway zone between the Kern plateau and a SE Sierra extensional domain (Figure 8).

5.4. Sediment Ponding and Exhumation in the Walker-Edison Graben System

[28] Deeply weathered low-relief basement rocks lying between Walker basin and the Bear Mountain fault constitute the exhumed floor of an early to middle Miocene volcanic depression defined as the Walker graben (Figure 8). The southeast domain of the graben was occupied by the Cache Peak volcanic center. The west margin of the graben was bounded by the Breckenridge fault, which in its transition with the White Wolf fault was breached by a major river channel that has been interpreted as the ancestral course of the lower Kern River [*MacPherson*, 1978]. As the river exited the range its course was controlled by a narrow northwest trending structural depression defined here as the Edison graben (Figures 1 and 8). The remnants of the Pleistocene river channel run partly along the graben, and then turn southwestward across the northwest extension of the Edison fault where the fault descends into the subsurface. Erosional remnants of Neogene strata that lie ponded in the partially exhumed Edison graben lap eastward onto the floor of the Walker graben (Figure 1).

[29] The southwest walls of the Walker and Edison grabens are defined by the Bear Mountain and Edison faults, respectively. The Bear Mountain fault is a NW striking, southwest-side-up normal fault that terminates against the White Wolf fault (Figure 1). It forms an ~750 m northeast facing topographic front with modest erosional modification. The Edison fault is a NW striking southwest-side-up normal fault that merges eastward with the northeast end of the White Wolf fault (Figure 1). It lies buried in the subsurface for much of its length. Stratigraphic and structural relations across the Edison fault suggest normal displacement of ~2000 m, with growth possibly initiating in the early to middle Miocene [*Dibblee and Warne*, 1986]. The northeast wall of the Edison graben is defined by a set of NW striking northeast-side-up normal faults that have undergone erosional modification. Both the Edison and Bear Mountain faults experienced ground breakage with minor vertical displacements during the 1952, M = 7.1 Arvin-Tehachapi earthquake [*Wood and Dale*, 1964; *San Joaquin Nuclear Project*, 1975].

[30] Apatite He ages from the Edison and Walker grabens are distinct from all other ages of the study area. They either show pronounced dispersion in replicate analyses (samples 56, 58, 59 and 61), or are anomalously young with well-constrained middle Miocene ages (samples 57 and 60). The age dispersion patterns are, for the most part, typical of patterns indicative of differential disturbance as a function of effective U concentration due to thermal blanketing by sediment burial [*Shuster et al.*, 2006; *Flowers et al.*, 2007]. Plots showing age dispersion as a function of effective U concentration are presented in Figure S2. Samples 56, 58, 59 and 61 once lay beneath graben fills in hanging walls of their respective graben bounding normal faults. Sample 60 lies in the footwall of the Edison fault. The footwall block continues westward into the margin of the Maricopa subbasin where it is abruptly covered by a thick Neogene marine section [*California Department of Oil and Gas*, 1967]. We interpret the 16.8 ± 0.4 Ma age for sample 60 to reflect rapid exhumation along the footwall of the Edison fault during growth faulting. Sample 57 lies along the deepest areas of the dissected floor of the Walker graben. We interpret its 14.8 ± 0.3 Ma age as recording complete resetting and subsequent rapid exhumation from beneath the deeper portions of the Walker graben sediment fill.

[31] Two samples were collected up the steep escarpment of the Bear Mountain fault (samples 62 and 63). The age variation with elevation is unusual (Table 1) as the highest elevation sample (63) is younger than the sample (62) located ~400 m below it. The inversion of the age-elevation relationship suggests southwest tilting. Assuming that in this area the apparent exhumation rate is also 0.06 mm/yr, a 12–20° southwest tilt is deduced, taking into account the age uncertainty. Such tilting is close to, but higher than the relatively gentle topographic slope (~12°) off the southwest flank of Bear Mountain. If this tilt resulted from normal displacement on the Bear Mountain fault it would correspond to 450–760 m vertical displacement, which is consistent with the 750 m northeast facing escarpment along the fault. Furthermore, Miocene strata that rest nonconformably on the southwest sloping basement of Bear Mountain dip 10–18°SW as they descend into the Tejon Platform (Figure 1) [*Dibblee et al.*, 1965]. Accessibility constraints prohibited the collection of additional samples along the sloping basement surface. The coincidence of the tilt implied by the limited footwall apatite He data and nonconformably overlying Miocene section, in conjunction with the geomorphic relations lead us to tentatively interpret Bear Mountain as a southwest tilted fault block controlled by normal displacement on the Bear Mountain fault.

[32] Subsurface relations indicate that during the Miocene the White Wolf fault acted as a transfer zone that partitioned differential extension along NW striking normal faults between the Maricopa subbasin to the northwest and the Tejon Platform to the southeast (Figure 1) [*MacPherson*, 1978; *Hirst*, 1986; *Goodman and Malin*, 1992]. This transfer zone continued northward as the Breckenridge–Kern Canyon zone, which bounded the western margin of

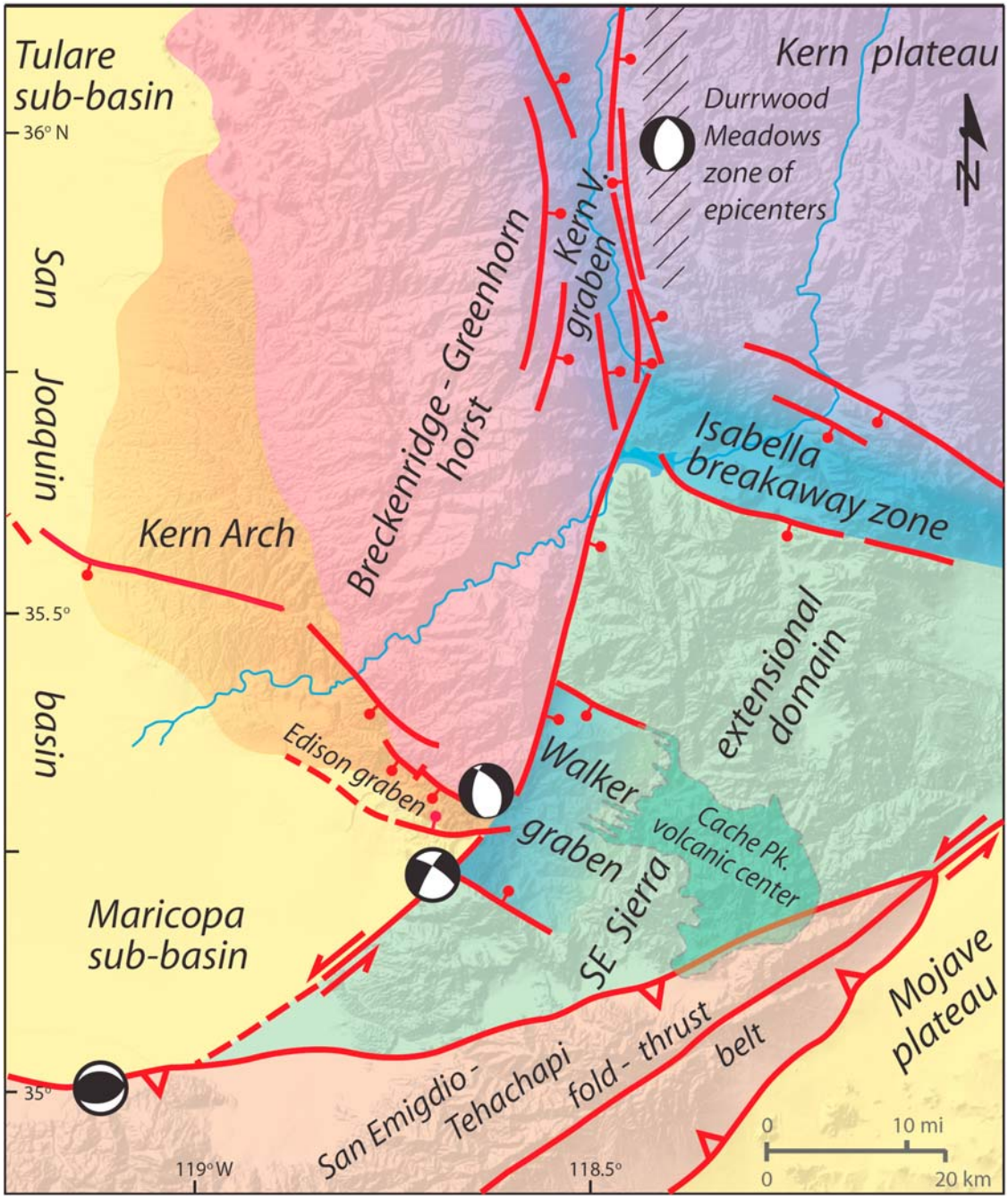

Figure 8. Tectonic domain map for late Cenozoic of southern Sierra Nevada–eastern San Joaquin basin region based on Figure 1 and analysis in text. Selected faults are shown which in part define domains. Thrust symbols denote mainly blind structures. Epicenters and focal mechanisms for major events are from *Jones and Dollar* [1986] and *Clinton et al.* [2006], with black areas representing compressional nodes.

the Isabella breakaway zone and the SE Sierra extensional domain (Figure 8).

6. Relationships With Sedimentation and Faulting in the Eastern San Joaquin Basin

[33] The continuity of the southern Sierra Nevada fault system into the eastern San Joaquin basin is demonstrated in Figure 1. Faults within the southern Sierra uplift record basement level deformation and exhumation, whereas those of the adjacent basin record cover strata levels of deformation and sedimentation. Structural and temporal relations of the faults from these two contrasting domains can thus be leveraged against one another to gain a fuller understanding of the tectonics of the system.

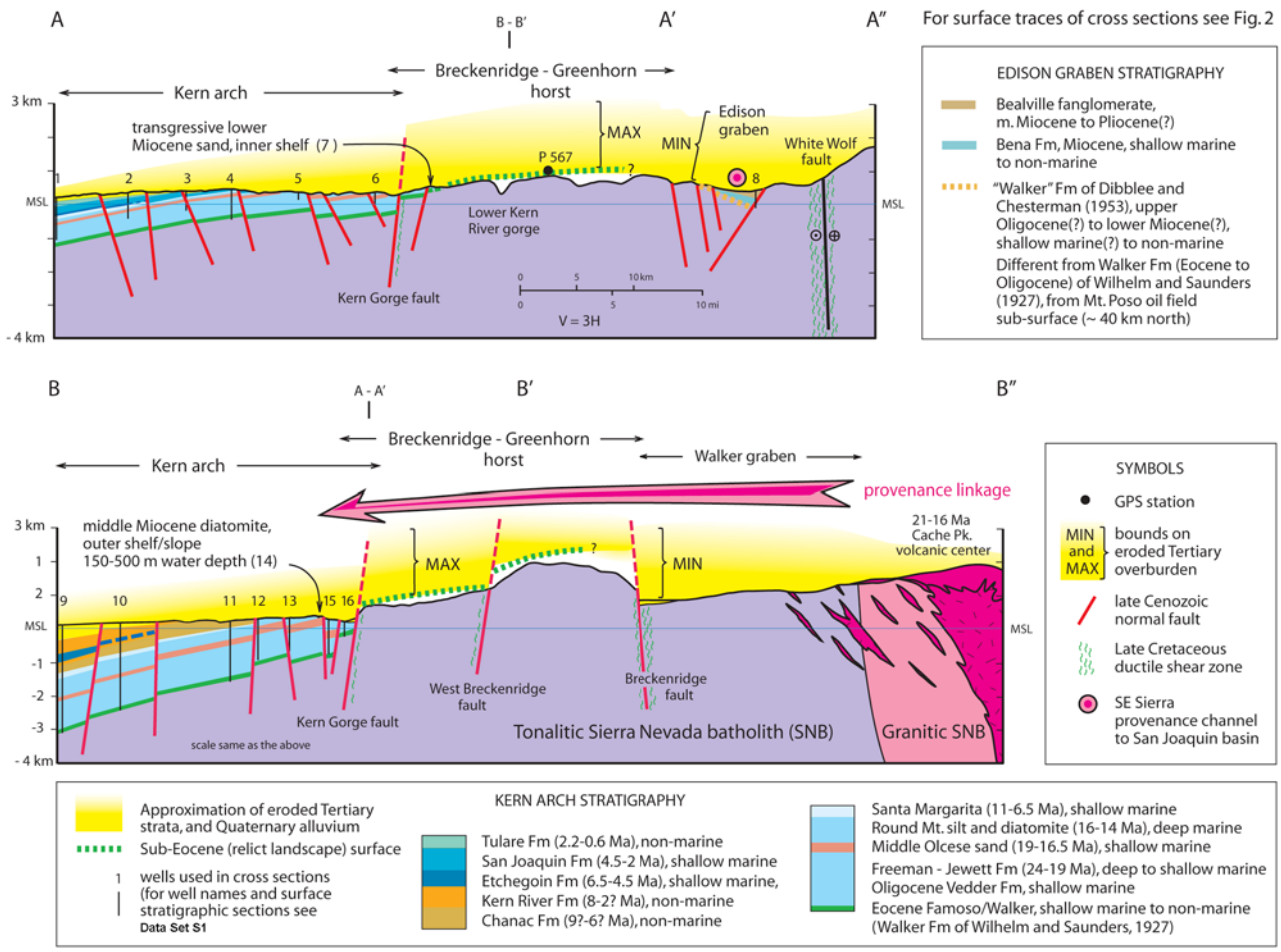

Figure 9. Cross sections across Kern arch and adjacent Sierra Nevada based on oil well data (Data Set S1) and Figure 1 structures. Yellow tone depicts approximate thickness of Tertiary strata eroded off arch, as well as maximum and minimum thicknesses eroded off adjacent Sierran basement based on apatite He age relations. Two possibilities are shown for exclusive delivery of eastern Sierra detritus to San Joaquin basin: (top) channeling through Breckenridge–White Wolf fault transition along Edison graben and/or (bottom) overtopping of Breckenridge fault as Walker graben filled.

6.1. Structural Framework of the San Joaquin Basin

[34] The San Joaquin basin is a distinct late Cenozoic depocenter that has developed along the southern ~100 km of the Great Valley [*Bandy and Arnal*, 1969]. In the late Oligocene through middle Miocene the paleoshoreline extended along a WNW–ESE trace across the Great Valley from the paleo-Sierra Nevada at latitude ~36°N, and a shelf environment sloped to the SSW and dropped into a deep marine basin [cf. *Bandy and Arnal*, 1969; *Addicott*, 1970; *Bartow*, 1984; *Olson*, 1988; *Bloch*, 1991]. The eastern limits of this basin are ill defined adjacent to the Sierra range front. Its southern limits were in part controlled by growth faulting along the White Wolf fault [*Goodman and Malin*, 1992], but are otherwise destroyed by the late Pliocene-Quaternary emergence of the San Emigdio-Tehachapi fold-thrust belt (Figure 8) [*Nilsen et al.*, 1973; *Davis and Lagoe*, 1988].

[35] The SSW deepening pattern of the San Joaquin basin is defined by lithofacies and biofacies relations as well as isopach patterns [*Simonson*, 1958; *Bandy and Arnal*, 1969; *Addicott*, 1970; *Bloch*, 1991]. This pattern has been overprinted by Quaternary rise of the Kern arch, as recorded in densely spaced well logs of the area [*California Department of Oil and Gas*, 1952, 1957, 1963, 1965, 1967]. The Kern arch is a broad normal fault controlled uplift that has partitioned the San Joaquin basin into the Maricopa subbasin to the south, and the Tulare subbasin to the north (Figure 8). The persistence of marine conditions across the Kern arch into late Pliocene time [*Klausing and Lohman*, 1964; *Lofgren and Klausing*, 1969] (Figure 9, cross section AA′A″) indicates its rise and emergence in the Quaternary. The Kern arch constitutes the lower elevation cover strata levels of the Breckenridge-Greenhorn horst. The southern Sierra fault system extends into and constitutes the principal structures cutting the arch as well as the Maricopa subbasin. Such structures are of great interest for in the area of the arch they form the principal petroleum trap structures.

6.2. Relationships Between the Kern Gorge and Pond-Poso Faults

[36] Geometric and offset relations indicate that the Kern Gorge and Pond-Poso faults are linked. The Kern Gorge fault passes into the subsurface of the Kern arch ~8 km to the northwest of the Kern River's exit of the range. In this area the geomorphic expression of the fault is subdued by a series of subsidiary normal faults that form a small graben (Figure 1). Subsurface data from the area of the graben indicate ~600 m east-side-up displacement on the Kern Gorge fault (Figure 9, AA′A″), which is similar to that determined above for its escarpment to the southeast. The Pond-Poso fault extends from the area of the graben at least 50 km NW, as it descends into the San Joaquin basin (Figure 1). Its apparent southeast termination consists of a dispersed zone of faulting and distributed brittle shear that continues into the area where the Kern Gorge fault descends into the graben. There is an ~25° discordance between the two faults, but nevertheless displacement patterns are consistent with the two being closely linked. Subsurface and trenching data from the Pond-Poso fault indicate growth faulting over the past ~1 Ma with a total northeast side up normal displacement of ~725 m, including modest Holocene activity [*San Joaquin Nuclear Project*, 1975; *Guacci and Purcell*, 1978]. This is very similar to that of the Kern Gorge fault, including evidence for Holocene displacement, which is consistent with the fresh scarp along the Kern Gorge range front.

6.3. Relationships Between the Breckenridge-Greenhorn Horst and the Kern Arch

[37] The Kern arch is an actively growing topographic promontory that extends westward into San Joaquin basin centered at latitude ~35.6°N (Figures 1 and 8). It is extensively faulted, yet its underlying Tertiary section forms a west dipping homocline. The extension of the upper Pliocene marine San Joaquin Formation from the Tulare subbasin southwards across an extensive area of the arch indicates uplift primarily in Quaternary time (Figure 9, AA′A″). At least 1 km of Tertiary strata have been eroded off the arch. Normal faults and related small grabens are widespread across the arch [*Nugent*, 1942], much more densely distributed than that shown on Figures 1 and 9. Regardless of its intensely faulted state the Tertiary section in general maintains an ~5–7° west dip [*California Department of Oil and Gas*, 1952, 1957, 1963; *Dibblee et al.*, 1965]. The basement surface beneath the arch has a comparable west slope, but with considerable local relief [*Wentworth et al.*, 1995]. The west slope of the basement surface continues upslope as the ~9° west tilt of the relict landscape surface across the Breckenridge-Greenhorn horst (Figure 9).

[38] The Kern arch constitutes the lower slope of the Breckenridge-Greenhorn horst, but with Tertiary cover strata remaining on the arch. Figure 9 (cross section BB′B″) shows the relations between the horst and the arch. Both constitute a regional west tilted block linked to the west side up motion on the Breckenridge and related faults. In Figure 9 (cross section AA′A″) the sub-Eocene nonconformity surface is shown continuing as the relict landscape surface across flat-topped interfluves southeastward to its disruption by normal faults that bound the Edison graben. Permanent GPS station P567 lies on the surface above the lower Kern River gorge. It records mm/yr scale uplift relative to Isabella basin and to the Tulare and Maricopa subbasins (Text S1), which is consistent with the horst/arch being an actively growing structure.

[39] Quaternary uplift of the Breckenridge-Greenhorn horst has resulted in the incision of the steep lower Kern River gorge. Sharp channel gradient changes with concave upward profiles across the Kern Gorge and west Breckenridge faults indicate that the channel has not yet fully adjusted to tectonically induced changes in local base level. Despite the steepness of the channel, and its incision into coherent basement, the channel possesses numerous sharp meanders. These meanders have wavelengths and amplitudes that resemble the lower stretches of the Kern River where it is incising through Tertiary strata of the arch (Figure 1). The lower Kern River gorge is interpreted as a superimposed valley with its meander forms inherited from its initial incision through the eroded Tertiary section.

6.4. Original Extent of San Joaquin Basin Across the Southern Sierra Nevada

[40] Resolution of the relict landscape surface across the Breckenridge-Greenhorn horst as well as facies and provenance relations in strata of the eastern San Joaquin basin indicate that the basin margin extended across part of the modern southern Sierra uplift. Stratigraphic and paleontologic studies indicate that littoral to bathyal conditions existed in immediate proximity to the current range front for much of Oligocene-Miocene time with littoral to supralittoral facies following in the late Miocene-Pliocene [*Addicott*, 1965, 1970; *Bandy and Arnal*, 1969; *Bartow*, 1984; *Bartow and McDougall*, 1984; *Olson*, 1988; *Bloch*, 1991; *Baron et al.*, 2007]. Backstripping calculations show that the crest area of the Kern arch was primarily under tectonic subsidence for late Oligocene through Miocene time [*Olson*, 1988], and well core and log data as well as surface mapping show that the area of the northern arch was under marine conditions in the late Pliocene [*Lofgren and Klausing*, 1969; *Klausing and Lohman*, 1964] (Figure 9, cross section AA′A″). Continuity of the Neogene section down to Eocene strata across much of the arch further indicates that the Cenozoic section rested in succession above the same sub-Eocene surface that is preserved as the relict landscape surface preserved across the Breckenridge-Greenhorn horst (Figure 9). The extent to which the Tertiary section extended directly across the area of the horst and into the Walker graben prior to the rise of the horst is poorly constrained.

[41] Provenance studies of upper Miocene-Pliocene fluvial strata exposed along the crest and southern slope of the Kern arch reveal an absence of clasts derived from tonalitic units that constitute basement of the Breckenridge-Greenhorn horst [*Saleeby et al.*, 2008]. Moreover, the only western Sierra detritus observed as of yet in the entire Cenozoic section of the arch are locally derived debris flows within the Edison graben, basal conglomerates lying on the sub-

Eocene surface, and late Quaternary fans shed from range front faults. Otherwise, clast populations are dominated by granites, granodiorites and Neogene volcanic rocks, all of which are typical of the eastern margin of the Walker graben and the Cache Peak volcanic center. These relationships indicate that during the deposition of the Tertiary section neither the Kern Gorge nor the west Breckenridge faults possessed enough structural relief to expose their footwall basement rocks. The provenance data also limits the amount of structural relief on the Breckenridge fault prior to Quaternary time, or implies the overtopping of detritus across the fault as the Walker graben filled. Figure 9 (cross section BB′B″) depicts this relationship in principal. This accounts for relatively deep burial of the Miocene Breckenridge fault hanging wall, resulting in apatite He age disturbances, and relatively shallow burial of the relict landscape surface across the horst, preserving the older apatite He ages. Downhole temperature measurements in the San Joaquin basin indicate highly variable thermal gradients [*California Department of Oil and Gas*, 1992]. Gradients are as high as 72°C/km on the Kern arch, and as low as 10°C/km in actively subsiding parts of the basin, reflecting nonequilibration due to rapid uplift and subsidence, respectively. Temperature gradients measured in fields located at the transition of the arch into the basin are similar to the ∼26°C/km regional thermal gradient modeled for the southwestern Sierra Nevada batholith [*Brady et al.*, 2006]. Using this value coupled with annual mean surface temperatures of ∼18°C for the region (U.S. Weather Bureau, NOAH data), no more than ∼2.2 km of strata covered the Breckenridge-Greenhorn horst prior to their erosion (Figure 9). The apatite He age disturbance patterns of samples taken from the floor of the Walker and Edison grabens, in contrast, indicate either ≥2.2 km of strata covered those areas, or if less, thermal gradients were higher due to volcanism and associated hypabyssal activity. This sediment overburden is consistent with the minimum thickness of ∼2.5 km for the partly eroded section of the Edison graben [*Dibblee and Warne*, 1986]. An alternative to the overtopping interpretation for the Miocene Breckenridge fault is that the eastern Sierra detritus was channeled through the area of the Edison graben and dispersed to the north and west into the San Joaquin basin (Figure 9, cross section BB′B″).

7. Discussion

7.1. Southern Sierra Nevada Fault System and Its Late Cenozoic Phases of Activity

[42] Two sets of normal and related transfer faults are resolved in the study area by a combination of field techniques and apatite He thermochronometry. These faults are known to have been active in the late Cenozoic from their geomorphic expressions, relationships with Neogene volcanic rocks, and by stratigraphic relations within the eastern San Joaquin basin. The faults that we resolve are the principal members of a much more extensive structural system characterized by additional faults, fault sets and lineaments, and small offset shears and tensile fractures that pervade the region. The two principal sets of this system may be distinguished as ∼NW and ∼N−S striking. Faults of the NW set commonly terminate against the N−S set. Some faults from each set exhibit fresh scarps and coseismic ground breakage, while others form topographic fronts lacking evidence of late Quaternary activity. The available age constraints suggest two distinct late Cenozoic phases of activity, early to middle Miocene and late Pliocene(?)-Quaternary. The early to middle Miocene episode was accompanied by volcanism and fault controlled ponding of sediments in the areas of the Maricopa subbasin and Walker graben. During this phase the White Wolf−Breckenridge−Kern Canyon zone functioned as a transfer system by partitioning differential extension between the Maricopa subbasin/Edsion graben and the southeastern Sierra extensional domain (Figure 8). Whether or not such a kinematic regime extended into the late Miocene is poorly constrained.

[43] The late Pliocene(?)-Quaternary phase of activity is reflected in pronounced topographic fronts, some with fresh scarps and coseismic ground breakage, and by seismicity. Question regarding the late Pliocene initiation of this phase of faulting arises from the widespread occurrence of upper Pliocene marine and lower Quaternary lacustrine strata across the area of the northern arch, and by widely distributed faulting of these strata (Figure 9, cross section AA′A″). Provisional GPS vertical displacement data add further question by the fact that such interseismic motion could generate all of the relief of the Kern arch and the Breckenridge-Greenhorn horst over a 1 Myr time scale. Inspection of Figure 9 (cross section AA′A″) reveals that it is conceivable that upper Pliocene marine conditions extended across the footwalls of the Kern Gorge and west Breckenridge faults prior to the rise of the arch/horst. The results of well-constrained focal mechanism studies are consistent with the integrated fault kinematic pattern shown for the bounding structures on the coupled arch/horst (Figure 8) [*Jones and Dollar*, 1986; *Clinton et al.*, 2006]. The Durrwood Meadows seismic swarm parallels the Kern Canyon fault and yields west-side-up normal displacement focal mechanisms that are consistent with the normal displacement pattern resolved for the young scarps of the Kern Canyon fault. Active extension off the southwest margin of the horst is reflected by a normal displacement mechanism on a NW striking fault. Such extension translates into sinistral transfer motion along the White Wolf fault as exhibited in the sinistral mechanism on a steep NE striking fault. Blind thrusting rooting southwards beneath the San Emigdio−Tehachapi fold-thrust belt is documented by thrust mechanisms further west along the "White Wolf" zone. The seismicity and GPS data along with ground breakage and fresh scarp relations clearly document the active role of the southern Sierra fault system in generating structural and topographic relief of the geologically young Kern arch and Breckenridge-Greenhorn horst.

7.2. Tectonics of Neogene-Quaternary Faulting of the Southern Sierra Nevada Region

[44] A number of researchers have suggested that Neogene faulting, subsidence and volcanism in the San

Joaquin basin and southern Sierra Nevada region resulted from the northward migration of the Mendocino triple junction during the inception of the San Andreas transform juncture [*Graham and Williams*, 1985; *Loomis and Glazner*, 1986; *Graham et al.*, 1989; *Goodman and Malin*, 1992]. Plate reconstructions for the Cenozoic of California place the northward trajectory of the triple junction along southern Sierra latitudes between 28 and 19 Ma [*Atwater and Stock*, 1998]. The reconstructions indicate that during this time interval a slab window progressively opened beneath the southern Sierra region as the triple junction migrated northward. We infer that it was the slab window, as opposed to the triple junction, that drove crustal extension, basin subsidence and volcanism. It is the infill of asthenosphere into the window that can conceivably account for all of the defining features of this tectonic regime.

[45] The geometry and kinematics of the southern Sierra Nevada fault system and its continuation into the San Joaquin basin are a unique response to triple junction migration and slab window opening along central California. Comparable structures are not present in the Sierran microplate north of latitude ~36°N. Furthermore, temporally and kinematically comparable faulting has not been recognized in the adjacent northwestern Mojave Desert region; nor in the northern Salinia domain which was displaced from the southern Sierra–San Joaquin basin region by late Miocene to Holocene motion on the San Andreas fault. Lower to middle Miocene strata that were deposited immediately east of the southeastern Sierra record minimal north–south extension [*Loomis and Burbank*, 1988]. Such extension may be related to that of the southern Sierra fault system, but its low strain magnitude only accent that which is recorded in the study area as unique. Neogene extensional faulting in the central Mojave Desert was restricted to east directed detachment faulting, which stepped southeastward into the southeastern California region [*Walker et al.*, 1990; *Martin et al.*, 1993; *Glazner et al.*, 1996].

[46] Structural and fabric studies in conjunction with medial to high temperature thermochronometric data (≥200°C) reveal that important members of the southern Sierra Nevada fault system formed in Late Cretaceous time in conjunction with the rapid deep exhumation of the southernmost Sierra Nevada batholith [*Saleeby et al.*, 2007; *Nadin and Saleeby*, 2008; J. Saleeby, unpublished data, 2009]. Thus Neogene displacements along the system are remobilizations. Analysis of the Late Cretaceous kinematics of the system reveals that the NW set acted as normal faults that cut rapidly exhumed footwall domains of larger south/southwest directed detachment faults that were instrumental in the exhumation of the deep-level rocks (~35 km) of the batholith [*Wood and Saleeby*, 1997; *Saleeby*, 2003]. As was the case for the Neogene phase of displacement, the Kern Canyon and proto-Breckenridge–White Wolf zone acted as strike-slip transfer structure between differentially extending domains. The driving tectonics for this Late Cretaceous tectonic regime was the segmentation of the subducting Farallon plate into a shallow megathrust flat that removed the mantle lithosphere from beneath the southernmost Sierra and adjacent Mojave Desert region. The most straight forward interpretation of the Neogene displacement history of the system is that the crust had been severely weakened by the Late Cretaceous phase of extensional faulting, as well as by the removal of the underlying mantle lithosphere, and when the slab window grew beneath the region the overlying crust extended passively. As the slab window migrated north of the Late Cretaceous damage zone its local structural and thermal expressions diminished as it encountered the structurally coherent residual Sierran mantle lithosphere.

[47] Late Miocene time presented a different tectonic regime in the southern Sierra region, as compared to earlier Miocene time. Sinistral displacement along the Garlock fault commenced, and the consolidation of the eastern Sierra escarpment system instigated the microplate behavior of the coupled Sierra Nevada and Great Valley producing the regional west tilt pattern [*Loomis and Burbank*, 1988; *Monastero et al.*, 1997; *Henry and Perkins*, 2001; *Mahéo et al.*, 2004; *DeOreo et al.*, 2005; *Rood et al.*, 2005]. Late Pliocene to Holocene time in the region is further distinguished by the delamination of the residual mantle lithosphere that was left truncated beneath the study area by the Late Cretaceous segmentation of the Farallon plate [*Saleeby et al.*, 2003; *Zandt et al.*, 2004; *Le Pourhiet et al.*, 2006]. The surface deformational response in the study area was the rise of the coupled Breckenridge-Greenhorn horst and Kern arch, and renewed normal faulting along both the NW and N–S fault sets. The west tilt of the horst is of the same sense as that of the greater Sierra Nevada to the north, except the controlling structures are the Breckenridge–Kern Canyon–Greenhorn faults, versus the eastern Sierra escarpment system. Our apatite He data do not support a west tilt derived from eastern escarpment faulting, south of latitude 36°N. In contrast, south of latitude 36°N, geomorphic as well as apatite He data indicate that the relict landscape surface east of the Kern Valley graben slopes southwards through the Kern plateau to the Isabella breakaway zone, south of where it is disrupted by extensional structures (Figure 8). Thus at present the controlling structure for the west tilt of the microplate south of latitude 36°N steps westward from the eastern Sierra escarpment to the Breckenridge–Kern Canyon zone. Geomorphic observations suggest that this transition may begin as far north as 36.5°N, which is also the latitude where the Kern Canyon scarps die out [*Saleeby et al.*, 2009]. The amount and temporal relations of tilt also change across this transition in that the entire Tertiary section of the Kern arch dips ~5–7°, whereas to the north tilts are progressive with age ranging from ~1° for Pliocene strata and only up to ~5° for Eocene strata [*Unruh*, 1991]. North of latitude ~36°N, the tilt of the Kern arch is distorted northward into the Tulare subbasin which forms an anomalous zone of late Pliocene-Quaternary subsidence, relative to the rest of the Great Valley, that has embayed into the western edge of the Sierran uplift [*Saleeby and Foster*, 2004; *Saleeby et al.*, 2009].

[48] The rise of the Kern arch and Breckenridge-Greenhorn horst closely followed the initiation of accelerated subsi-

dence in the adjacent Tulare subbasin. The Tulare subbasin sits above a vertical high density mass in the upper ~225 km of the mantle that is interpreted as foundered mantle lithosphere, whereas the arch/horst sits above thinner crust that is underlain by low velocity uppermost mantle [*Fliedner et al.*, 2000; *Zandt et al.*, 2004]. Our working model for the driving mechanism of the surface motions of the Tulare subbasin and the uplift/horst is viscous coupling of subbasin subsidence to the descending high-density mass coupled to buoyancy driven uplift around the basin periphery in response to asthenosphere ascent into the space vacated by the foundered mantle lithosphere [cf. *Pysklywec and Cruden*, 2004; *Le Pourhiet et al.*, 2006]. This in theory also accounts for the encroachment of late Pliocene marine conditions across the areas of the Kern arch, and very likely the recently exhumed adjacent western Sierra (Figure 9, cross section AA′A″). Upper mantle buoyancy driven epeiorgenic uplift is consistent with low-magnitude extension on roughly rectilinear normal fault sets, which is also consistent with regional stress field inversions from seismicity of the southern Sierra region indicating that the upper crust is undergoing brittle oblate extensional flattening as it is rising [*Unruh and Hauksson*, 2009]. We posit that the preweakened state of the crust arising from earlier extensional tectonic regimes was highly instrumental in promoting the current phase of faulting within this essentially epeiorgenic deformation field.

7.3. Relations Between the Relict Landscape Surface and the Eocene Basal Nonconformity of the Eastern San Joaquin Basin

[49] Continuity between the relict landscape surface and the Eocene basal nonconformity of the eastern San Joaquin basin, between latitudes 35.5°N and 36°N (Figures 1 and 9), indicate that these surfaces are one and the same. Strict equivalence of these surfaces, in theory should break down eastward as a function of whether or not Tertiary cover strata rested on the surface, and if so for what duration they have been removed. In areas where cover strata have been stripped off the surface subsequent erosional modification, in theory, has progressed at ~0.06 mm/yr, the apparent exhumation rate for the region as determined above. We have used the relict landscape surface as a critical datum in our analysis of the distribution of the apatite He ages, and in linking southern Sierra Nevada structural and landscape evolution to the structure and stratigraphy of the eastern San Joaquin basin. In addition to the specific ties that we have made between the landscape surface and basin stratigraphy, we recognize regional parallels in the nature of the relict surface and basal relations of the eastern San Joaquin basin section.

[50] Geomorphic analysis and apatite He data for the axial to eastern domains of the southern Sierra Nevada show that the relict landscape surface changes at latitude ~36.5°N from its regional WSW tilt to a south tilt that continues southwards until its disruption at the Isabella breakaway zone (Figure 8). From the breakaway zone southward the surface is structurally disrupted and for the most part irresolvable. Inspection of Digital Elevation Models reveals a change in the landscape to more pronounced local relief across the extended domain (Figure 1). The change in the regional slope of the basement surface at ~36.5°N mimics the southerly slope of the San Joaquin basin, prior to the rise of the Kern arch, as the basin was superimposed across earlier regional stratigraphic trends of the Great Valley. This is visible from the total thickness variations in the two cross sections of Figure 9. Basal relations along the eastern San Joaquin basin also mimic the southward disruption of the relict surface as observed across the SE Sierra extensional domain. From the area of the Kern River's exit of the range northward the base of the Tertiary section is defined by Eocene and local Paleocene units (Figure 9). Locally derived western Sierra detritus are not observed in these units except locally along the basal nonconformity. In contrast, from the southwest slopes of Breckenridge Mountain to the area of the Edison fault, and extending into the Walker graben floor the base of the section is upper Oligocene(?)-lower Miocene, and local basement-derived clastic strata sourced from active fault scarps are abundant within the section [*Bartow and McDougall*, 1984; *Dibblee and Warne*, 1986] (also our data). Such north to south changes in the basal relations of the Tertiary section arose from the early Neogene phase of faulting along the southern Sierra system, just as the changes in Sierran landscape across the Isabella breakaway zone did. These relations demonstrate how closely aligned the tectonics and landscape development of the southern Sierra Nevada was with the tectonics and sedimentation patterns of the eastern San Joaquin basin.

8. Conclusions

[51] We have used apatite He thermochronometry to resolve the orientation of the regional paleohorizontal that existed during wide spread cooling of the southern Sierra Nevada batholith, following abrupt termination of magmatism in the Late Cretaceous. Prior work [*Clark et al.*, 2005] defined a critical regional datum within this paleohorizontal space by resolution of the slowly exhuming surface of the batholith that evolved into a relict low relief landscape surface during the Cenozoic. The thermochronometric mapping of the surface between 35.2°N and 36°N in conjunction with geomorphic and structural studies resolve a system of normal and related transfer faults that were active in the Neogene, some of which have remained active, or were remobilized in the Quaternary. Subsurface mapping in the adjacent San Joaquin basin indicates that the system penetrates the basin, and controlled subsidence in the Maricopa subbasin. The two principal fault sets of the system trend ~N–S and ~NW, with the NW set commonly terminating against the N–S set. A number of these faults represent remobilizations along Late Cretaceous ductile to brittle shear zones. Most significant of these is the ~N–S Kern Canyon zone, which bends southwestward and continues as the White Wolf zone. The first resolvable remobilization of this integrated zone was in the early Neogene when it acted as an oblique transfer system that partitioned extension across the NW fault set in the southeastern Sierra from

similar oriented extension in Maricopa subbasin to the west. The transfer system also underwent vertical displacements that contributed to the ponding of sediments and volcanics in the subbasin as well as within the Walker graben of the southeastern Sierra. Facies and provenance relations within the eastern San Joaquin basin in conjunction with the mapping of the relict landscape surface into continuity with the Eocene basal nonconformity of the basin indicate that the eastern margin of the Neogene basin lay east of the current range front in continuity with strata ponded within the Walker graben.

[52] In the late Pliocene and Quaternary the southern Sierra Nevada underwent a phase of accelerated uplift in response to the delamination of the underlying mantle lithosphere. West-side-up normal displacement on the integrated Kern Canyon–Breckenridge and related faults resulted in ~9° west tilt on the relict landscape surface to the west, continuing westward to a comparable west dip imparted onto strata of the eastern San Joaquin basin. This faulting was accompanied by NE side up displacements on NW striking normal faults which both bound the northeast margin of Maricopa subbasin and terminate against the southern end of the Kern Canyon–Breckenridge zone. This fault geometry resulted in the northwest widening wedge shaped Breckenridge-Greenhorn horst. The Tertiary section was eroded off the upper slopes of the horst, with the ensuing incision of the lower Kern River Gorge, whereas along its lower slopes actively eroding Tertiary strata remain as the Kern arch. In its area of highest structural relief the arch has had at least 1 km of its Tertiary section eroded off. Erosion of $\leq$2.2 km of strata off the relict landscape surface lying on the horst is in accord with the apatite He ages determined along that portion of the surface retaining their Late Cretaceous signals. Ponding and subsequent erosion of $\geq$2.2 km of strata from the floor of the Walker graben is in accord with apatite He age disturbance patterns of samples from the exhumed floor of the graben.

[53] The southern Sierra fault system and its continuation into the San Joaquin basin are unique to the Sierra Nevada microplate. Elsewhere, for ~500 km to the north, the microplate is behaving as a rigid body progressively tilting westward with uplift and erosion balanced by subsidence and sedimentation in the Great Valley. Neogene faulting, basin subsidence and volcanism of the southern Sierra–San Joaquin basin are readily equated in time with the passage of the Mendocino triple junction and the opening of a slab window. The reason for the lack of such features not having developed in the greater microplate to the north as the slab window migrated northward may be explained by the fact that the southern Sierra fault system was preexisting. The Late Cretaceous structural system that the Neogene-Quaternary faults preferentially developed along is restricted to the same region as the Neogene-Quaternary faulting. This suggests that both during the early Neogene opening of the underlying slab window, and during the late Pliocene-Quaternary delamination of the underlying mantle lithosphere, the previously disrupted batholithic crust of the region underwent passive extension along mainly preexisting structures in response to upper mantle induced epeiorgenic forces.

[54] **Acknowledgments.** This research was supported by NSF grants EAR-0230383 and EAR-0606903 and funds from the Gordon and Betty Moore Foundation. We thank Elisabeth Nadin, Marin Clark, and Janice Gillespie for helpful discussions and assistance in the field and Lindsey Hedges for analytical assistance. Helpful reviews by George Hilley and John Wakabayashi are gratefully acknowledged. G. Mahéo benefited from the Lavoisier Post-Doctoral Fellowship. Caltech Tectonics Observatory contribution 85.

References

Addicott, W. O. (1965), Miocene macrofossils of the southeastern San Joaquin Valley, California, *U.S. Geol. Surv. Prof. Pap.*, *525-C*, 101–109.

Addicott, W. O. (1970), Miocene Gastropods and biostratigraphy of the Kern River area, California, *U.S. Geol. Surv. Prof. Pap.*, 642, 174 pp.

Argus, D. F., and R. G. Gordon (1991), Current Sierra Nevada–North America motion from very long baseline interferometry: Implications for the kinematics of the western United States, *Geology*, *19*, 1085–1088, doi:10.1130/0091-7613(1991)019<1085:CSNNAM>2.3.CO;2.

Atwater, T., and J. Stock (1998), Pacific–North American plate tectonics of the Neogene southwestern United States: An update, in *Integrated Earth and Environmental Evolution of the Southwestern United States*, edited by W. G. Ernst and C. A. Nelson, pp. 393–420, Bellwether, Columbia, Md.

Bandy, O. L., and R. E. Arnal (1969), Middle Tertiary basin development, San Joaquin Valley, California, *Geol. Soc. Am. Bull.*, *80*, 783–820, doi:10.1130/0016-7606(1969)80[783:MTBDSJ]2.0.CO;2.

Baron, D., R. M. Negrini, E. M. Golob, D. Miller, A. Sarna-Wojcicki, B. Fleck, B. Hacker, and A. Erendi (2007), Geochemical Correlation and $^{40}Ar/^{39}Ar$ dating of the Kern River ash bed related tephra layers: Implications for the stratigraphy of petroleum-bearing formations in the San Joaquin Valley, California, *Quat. Int.*, *178*, 236–260.

Bartow, J. A. (1984), Geologic map and cross sections of the southeastern margin of the San Joaquin Valley, California, *U.S. Geol. Surv. Misc. Invest. Ser.*, *Map I-1496*, scale 1:125,000.

Bartow, J. A., and K. McDougall (1984), Tertiary stratigraphy of the southeastern San Joaquin Valley, California, *U.S. Geol. Surv. Bull.*, *18*, *1529 J*, 41 pp.

Bloch, R. (1991), Studies of the stratigraphy and structure of the San Joaquin basin, Ph.D. dissertation, 319 p., Stanford Univ., Stanford, Calif.

Brady, R. J., M. N. Ducea, S. Kidder, and J. Saleeby (2006), The distribution of radiogenic heat production as a function of depth in the Sierra Nevada Batholith, California: A new approach to an old problem, *Lithos*, *86*, 229–244, doi:10.1016/j.lithos.2005.06.003.

Braun, J. (2002), Quantifying the effect of recent relief changes on age-elevation relationships, *Earth Planet. Sci. Lett.*, *200*, 331–343, doi:10.1016/S0012-821X(02)00638-6.

Burbank, D., and R. Anderson (2000), *Tectonic Geomorphology*, 270 pp., Blackwell Sci., Oxford, U. K.

California Department of Oil and Gas (1952), Kern River Field, in *Summary of Operations, California Oil Fields*, *Annu. Rep. State Oil Gas Supervisor 38*(2), Sacramento.

California Department of Oil and Gas (1957), Mount Poso Field, in *Summary of Operations, California Oil Fields*, *Annu. Rep. State Oil Gas Supervisor 43*(2), Sacramento.

California Department of Oil and Gas (1963), Round Mountain Field, in *Summary of Operations, California Oil Fields*, *Annu. Rep. State Oil Gas Supervisor 49*(2), Sacramento.

California Department of Oil and Gas (1965), Kern Front Field, in *Summary of Operations, California Oil Fields*, *Annu. Rep. State Oil Gas Supervisor 51*, (1), Sacramento.

California Department of Oil and Gas (1967), Edison Field, in *Summary of Operations, California Oil Fields*, *Annu. Rep. State Oil Gas Supervisor 52*(2), part 2, Sacramento.

California Department of Oil and Gas (1992), California Oil and Gas Fields, Canfield Ranch, Rosedale, Round Mountain and Stockdale fields, vol. 1, Sacramento.

Cecil, M. R., M. N. Ducea, P. W. Reiners, and G. C. Chase (2006), Cenozoic exhumation of the northern Sierra Nevada, California, from (U-Th)/He thermochronology, *Geol. Soc. Am. Bull.*, *118*, 1481–1488, doi:10.1130/B25876.1.

Clark, M. K., and K. A. Farley (2007), Sierra Nevada river incision from apatite $^{4}He/^{3}He$ thermochronometry, *Eos Trans. AGU*, *88*(52), Fall Meet. Suppl., Abstract T31E-03.

Clark, M. K., G. Maheo, J. Saleeby, and K. A. Farley (2005), The non-equilibrium landscape of the southern Sierra Nevada, California, *GSA Today*, *15*, 4–10, doi:10.1130/1052-5173(2005)015[4:TNLOTS]2.0.CO;2.

Clinton, J. F., E. Hauksson, and K. Solanki (2006), An evaluation of the SCSN moment tensor solutions: Robustness of the M_w magnitude scale, style of faulting and automation method, *Bull. Seismol. Soc. Am.*, *96*, 1689–1705, doi:10.1785/0120050241.

Coles, S., D. R. Prothero, J. P. Quinn, and C. C. Swisher III (1997), Magnetic stratigraphy of the middle Miocene Bopesta Formation, southern Sierra Nevada, California, in *Geology of the Western Cordilleran: Perspectives From Undergraduate Research*, edited by G. H. Girty, R. E. Hanson, and J. D. Cooper, *Spec. Publ. SEPM Soc. Sediment. Geol.*, *82*, 21–34.

Davis, T. L., and M. B. Lagoe (1988), A structural interpretation of major tectonic events affecting the western and southern margins of the San Joaquin Valley, California: Field Trip Guidebook, *Spec. Publ. Soc. Econ. Paleontol. Mineral.*, *60*, 65–87.

DeOreo, S. B., C. J. Busby, P. Gans, and I. Skilling (2005), Carson Pass-Kirkwood paleocanyon system: Implication for the Tertiary evolution of the Sierra Nevada, California, *Geol. Soc. Am. Abstr. Programs*, *37*(4), 65.

Dibblee, T. W., Jr., and A. H. Warne (1986), Inferred relation of the Oligocene to Miocene Bealville Fanglomerate to the Edison fault, Caliente Canyon area, Kern County, California, in *Studies of the Geology of the San Joaquin Basin*, pp. 223–232, Pac. Sect., Soc. of Econ. Paleontol. and Mineral., Upland, Calif.

Dibblee, T. W., Jr., W. G. Bruer, O. Hackel, and A. H. Warne (1965), Geologic map of the southeastern San Joaquin Valley (Kern River to Grapevine Canyon) Kern County, California, in *Geology of Southeastern San Joaquin Valley, California, Kern River to Grapevine Canyon*, edited by O. Hackel, pp. 25, Pac. Sect., Am. Assoc. of Pet. Geol., Los Angeles, Calif.

Edwards, E. C. (1943), Kern front area of the Kern River oil field, in *Geologic Formations and Economic Development of Oil and Gas Fields of California*, *Bull. Calif. Div. Mines Geol.*, *118*, 570–574.

Evernden, J. F., D. E. Savage, G. H. Gurnis, and G. T. James (1964), Potassium-argon dates and the Cenozoic mammalian chronology of North America, *Am. J. Sci.*, *262*, 145–198.

Farley, K. A. (2000), Helium diffusion from apatite: General behaviour as illustrated by Durango fluorapatite, *J. Geophys. Res.*, *105*, 2903–2914, doi:10.1029/1999JB900348.

Farley, K. A. (2002), (U-Th)/He dating: Techniques, calibrations, and applications, in *Noble Gases in Geochemistry and Cosmochemistry*, *Rev. Mineral. Geochem.*, vol. 47, edited by D. P. Porcelli, C. J. Ballentine, and R. Wieler, pp. 819–844, Mineral. Soc. of Am., Chantilly, Va., doi:10.2138/rmg.2002.47.18.

Fliedner, M. M., S. L. Klemperer, and N. I. Christensen (2000), Three-dimensional seismic model of the Sierra Nevada arc, California, and its implications for crustal and upper mantle composition, *J. Geophys. Res.*, *105*, 10,899–10,921, doi:10.1029/2000JB900029.

Flowers, R. M., D. L. Shuster, B. P. Wernicke, and K. A. Farley (2007), Radiation damage control on apatite (U-Th)/He dates from the Grand Canyon region, Colorado Plateau, *Geology*, *35*(5), 447–450, doi:10.1130/G23471A.1.

Gallagher, K., R. Brown, and C. Johnson (1998), Fission track analysis and its applications to geological problems, *Annu. Rev. Earth Planet. Sci.*, *26*, 519–572, doi:10.1146/annurev.earth.26.1.519.

Gilbert, G. K. (1928), Studies of Basin and Range structure, *U.S. Geol. Surv. Prof. Pap.*, *153*, 92 pp.

Glazner, A. F., J. M. Bartley, and R. V. Ingersol (1996), Collapse of southwestern North America and the evolution of early Miocene detachment faults, metamorphic core complexes, the Sierra Nevada orocline, and the San Andreas fault system: Comment and reply, *Geology*, *24*, 858–859, doi:10.1130/0091-7613(1996)024<0858:COSNAA>2.3.CO;2.

Goodman, E. D., and P. E. Malin (1992), Evolution of the southern San Joaquin Basin and mid-Tertiary transitional tectonics, central California, *Tectonics*, *11*, 478–498, doi:10.1029/91TC02871.

Graham, S. A., and L. A. Williams (1985), Tectonic, depositional, and diagenetic history of Monterey Formation (Miocene), central San Joaquin Basin, California, *AAPG Bull.*, *69*, 385–411.

Graham, S. A., R. G. Stanley, J. V. Bent, and J. B. Carter (1989), Oligocene and Miocene paleogeography of central California and displacement along the San Andreas fault, *Geol. Soc. Am. Bull.*, *101*, 711–730, doi:10.1130/0016-7606(1989)101<0711:OAMPOC>2.3.CO;2.

Guacci, G., and C. W. Purcell (1978), Evidence for middle Pleistocene and possible Holocene faulting on the Pond-Poso Creek fault, southern San Joaquin Valley, California, *Geol. Soc. Am. Abstr. Programs*, *10*(3), 108.

Henry, C. D., and M. E. Perkins (2001), Sierra Nevada-Basin and Range transition near Reno, Nevada: Two stage development at 12 and 3 Ma, *Geology*, *29*, 719–722, doi:10.1130/0091-7613(2001)029<0719:SNBART>2.0.CO;2.

Hirst, B. (1986), Tectonic development of the Tejon and adjacent areas, in *Structure and stratigraphy of the east side San Joaquin Valley, Guidebook*, edited by P. Bell, pp. 2–8, Pac. Sect., Am. Assoc. of Pet. Geol., Los Angeles, Calif.

Hoots, H. W., T. L. Bear, and W. D. Kleinpell (1954), Geological summary of the San Joaquin Valley, California, in *Geology of Southern California*, *Bull. Calif. Div. Mines Geol.*, *170*, 113–129.

House, M. A., B. P. Wernicke, K. A. Farley, and T. A. Dumitru (1997), Cenozoic thermal evolution of the central Sierra Nevada, from (U-Th)/He thermochronometry, *Earth Planet. Sci. Lett.*, *151*, 167–179, doi:10.1016/S0012-821X(97)81846-8.

House, M. A., B. P. Wernicke, and K. A. Farley (1998), Dating topography of the Sierra Nevada, California, using apatite (U-Th)/He ages, *Nature*, *396*, 66–69, doi:10.1038/23926.

House, M. A., B. P. Wernicke, and K. A. Farley (2001), Paleo-geomorphology of the Sierra Nevada, California, from (U-Th)/He ages in apatite, *Am. J. Sci.*, *301*, 77–102, doi:10.2475/ajs.301.2.77.

Jones, L. M., and R. S. Dollar (1986), Evidence of basin-and-range extensional tectonics in the Sierra Nevada; the Durrwood Meadows swarm, Tulare County, California (1983–1984), *Bull. Seismol. Soc. Am.*, *76*, 439–461.

Klausing, R. L., and K. E. Lohman (1964), Upper Pliocene marine strata on the east side of the San Joaquin Valley, California, *U.S. Geol. Surv. Prof. Pap.*, *475-D*, 14–17.

Le Pourhiet, L., M. Gurnis, and J. Saleeby (2006), Mantle instability beneath the Sierra Nevada Mountains in California and Death Valley extension, *Earth Planet. Sci. Lett.*, *251*, 104–119, doi:10.1016/j.epsl.2006.08.028.

Lofgren, B. E., and R. L. Klausing (1969), Land subsidence due to ground-water withdrawal, Tulare-Wasco area, California, *U.S. Geol. Surv. Prof. Pap.*, *437-B*, 103 pp.

Loomis, D. P., and D. W. Burbank (1988), The stratigraphic evolution of the El Paso basin, southern California: Implications for the Miocene development of the Garlock fault and uplift of the Sierra Nevada, *Geol. Soc. Am. Bull.*, *100*, 12–28, doi:10.1130/0016-7606(1988)100<0012:TSEOTE>2.3.CO;2.

Loomis, D. P., and A. F. Glazner (1986), Middle Miocene tectonic uplift of the southern San Joaquin Basin, California, *AAPG Bull.*, *70*, 1003–1007.

MacPherson, B. A. (1978), Sedimentation and trapping mechanism in upper Miocene Stevens and older turbidite fans of southeastern San Joaquin Valley, California, *Am. Assoc. Pet. Geol. Bull.*, *62*(11), 2243–2274.

Mahéo, G., K. A. Farley, M. K. Clark, and D. Shuster (2004), Cooling and exhumation of the Sierra Nevada Batholith in the Mount Whitney area (California) based on (U-Th)/He thermochronometry, *Eos Trans. AGU*, *85*(47), Fall Meet. Suppl., Abstract T41D-1252.

Mancktelow, N. S., and B. Grasemann (1997), Time-dependent effects of heat advection and topography on cooling histories during erosion, *Tectonophysics*, *270*, 167–195, doi:10.1016/S0040-1951(96)00279-X.

Martin, M. W., A. F. Glazner, J. D. Walker, and E. R. Schermer (1993), Evidence for right-lateral transfer faulting accommodating en echelon Miocene extension, Mojave Desert, California, *Geology*, *21*, 355–358, doi:10.1130/0091-7613(1993)021<0355:EFRLTF>2.3.CO;2.

Monastero, F. C., A. E. Sabin, and J. D. Walker (1997), Evidence for post-early Miocene initiation of movement on the Garlock fault from offset of the Cudahy Camp Formation, east-central California, *Geology*, *25*, 247–250, doi:10.1130/0091-7613(1997)025<0247:EFPEMI>2.3.CO;2.

Nadin, E. S. (2007), Structure and history of the Kern Canyon fault system, southern Sierra Nevada, California, Ph.D. thesis, 297 pp., Calif. Inst. of Technol., Pasadena.

Nadin, E. S., and J. B. Saleeby (2008), Disruption of regional primary structure of the Sierra Nevada batholith, California, in *Ophiolites, Arcs and Batholiths: A Tribute to Cliff Hopson*, edited by J. E. Wright and J. W. Shervais, *Spec. Pap. Geol. Soc. Am.*, *438*, 429–454, doi:10.1130/2008.2438(15).

Nilsen, T. H., T. W. Dibblee, and W. O. Addicott (1973), Lower and middle Tertiary stratigraphic units of the San Emigdio and western Tehachapi Mountains, California, *U.S. Geol. Surv. Bull.*, *1372-H*, H1–H23.

Nugent, L. E., Jr. (1942), The genesis of subordinate conjugate faulting in the Kern River salient, *J. Geol.*, *50*, 900–913, doi:10.1086/625090.

Olson, H. C. (1988), Middle Tertiary stratigraphy, depositional environments, paleoecology, and tectonic history of the southeastern San Joaquin Basin, California, Ph.D. dissertation, 353 pp., Stanford Univ., Stanford, Calif.

Pysklywec, R. N., and A. R. Cruden (2004), Coupled crust-mantle dynamics and intraplate tectonics: Two-dimensional numerical and three-dimensional analogue modeling, *Geochem. Geophys. Geosyst.*, *5*, Q10003, doi:10.1029/2004GC000748.

Rood, D. H., C. J. Busby, A. S. Jayko, and B. P. Luyendyk (2005), Neogene to Quaternary kinematics of the central Sierran frontal fault system in the Sonora pass region: Preliminary structural, paleomagnetic and neotectonic results, *Abst. Geol. Soc. Am. Abstr. Programs*, *4*, 65.

Ross, D. C. (1986), Basement–rock correlations across the White Wolf–Breckenridge–southern Kern Canyon fault zone, southern Sierra Nevada, California, *U. S. Geol. Surv. Bull.*, *1651*, 25 pp.

Saleeby, J. (2003), Segmentation of the Laramide slab-evidence from the southern Sierra Nevada region, *Geol. Soc. Am. Bull.*, *115*, 655–668, doi:10.1130/0016-7606(2003)115<0655:SOTLSF>2.0.CO;2.

Saleeby, J., and Z. Foster (2004), Topographic response to mantle lithosphere removal, southern Sierra Nevada region, California, *Geology*, *32*, 245–248, doi:10.1130/G19958.1.

Saleeby, J., M. Ducea, and D. Clemens-Knott (2003), Production and loss of high-density batholithic root, southern Sierra Nevada, California, *Tectonics*, *22*(6), 1064, doi:10.1029/2002TC001374.

Saleeby, J., K. Farley, R. W. Kistler, and R. Fleck (2007), Thermal evolution and exhumation of deep level batholithic exposures, southernmost Sierra Nevada, California, in *Convergent Margin Terranes and Associated Regions, a Tribute to W. G. Ernst*, edited by M. Cloos et al., *Spec. Pap. Geol. Soc. Am.*, *419*, 39–66, doi:10.1130/2007.2419(02).

Saleeby, J., M. N. Ducea, C. J. Busby, E. S. Nadin, and P. H. Wetmore (2008), Chronology of pluton emplacement and regional deformation in the southern Sierra Nevada, California, in *Ophiolites, Arcs and Batholiths: A Tribute to Cliff Hopson*, edited by J. E. Wright and J. W. Shervais, *Spec. Pap. Geol. Soc. Am.*, *438*, 397–428, doi:10.1130/2008.2438(14).

Saleeby, J., Z. Saleeby, E. Nadin, and G. Maheo (2009), Step-over in the structure controlling the regional west tilt of the Sierra Nevada microplate: Eastern escarpment system to Kern Canyon system, *Int. Geol. Rev.*, *51*(7), 634–669, doi:10.1080/00206810902867773.

San Joaquin Nuclear Project (1975), Early site review report, *report submitted to the U.S. Nuclear Regulatory Commission*, 5 vols., Dep. of Water and Power, Los Angeles, Calif.

Shuster, D. L., R. M. Flowers, and K. A. Farley (2006), The influence of natural radiation damage on helium diffusion kinetics in apatite, *Earth Planet. Sci. Lett.*, *249*(3–4), 148–161, doi:10.1016/j.epsl.2006.07.028.

Simonson, R. R. (1958), Oil in San Joaquin Valley, California, in *Habitat of Oil: A Symposium: Including Papers Presented at the Fortieth Annual Meeting of the Association, at New York, March 28–31, 1955*, edited by L. G. Weeks, pp. 99–112, Am. Assoc. of Pet. Geol., Tulsa, Okla.

Snyder, N. P., K. X. Whipple, G. E. Tucker, and D. Merritts (2000), Landscape response to tectonic forcing: DEM analysis of stream profiles in the Mendocino Triple Junction Region, northern California, *Geol. Soc. Am. Bull.*, *112*(8), 1250–1263, doi:10.1130/0016-7606(2000)112<1250:LRTTFD>2.3.CO;2.

Stock, G. M., R. S. Anderson, and R. C. Finkel (2004), Pace of landscape evolution in the Sierra Nevada, California, revealed by cosmogenic dating of cave sediments, *Geology*, *32*, 193–196, doi:10.1130/G20197.1.

Stüwe, L., R. White, and X. Brown (1994), The influence of eroding topography on steady-state isotherms: Application to fission-track analysis, *Earth Planet. Sci. Lett.*, *124*, 63–74, doi:10.1016/0012-821X(94)00068-9.

Unruh, J. R. (1991), The uplift of the Sierra Nevada and implications for late Cenozoic epeirogeny in the western Cordillera, *Geol. Soc. Am. Bull.*, *103*, 1395–1404, doi:10.1130/0016-7606(1991)103<1395:TUOTSN>2.3.CO;2.

Unruh, J., and E. Hauksson (2009), Seismotectonics of the southern Sierra Nevada-Walker Lane transition, eastern California, in *Late Cenozoic Structure and Evolution of the Great Basin-Sierra Nevada Transition*, edited by J. S. Oldow and P. H. Cashman, *Spec. Pap. Geol. Soc. Am.*, *447*, 351–372.

Walker, J. D., J. M. Bartley, and A. F. Glazner (1990), Large-magnitude Miocene extension in the central Mojave Desert: Implications for Paleozoic to Tertiary tectonics, *J. Geophys. Res.*, *95*, 557–569, doi:10.1029/JB095iB01p00557.

Wentworth, C. M., G. R. Fisher, P. Levine, and R. C. Jachens (1995), The surface of crystalline basement, Great Valley and Sierra Nevada, California: A digital map database, *U.S. Geol. Surv. Open File Rep.*, *95–96*.

Whipple, K. X. (2001), Fluvial landscape response time: How plausible is steady-state denudation?, *Am. J. Sci.*, *301*, 313–325, doi:10.2475/ajs.301.4-5.313.

Whipple, K. X., and G. E. Tucker (1999), Dynamics of the stream-power river incision model: Implications for height limits of mountain ranges, landscape response timescales, and research needs, *J. Geophys. Res.*, *104*, 17,661–17,674, doi:10.1029/1999JB900120.

Wilhelm, V. H., and L. W. Saunders (1927), Report on the Mt. Poso oil field (Kern County): California Oil Fields, *Publ. Calif. Div. Oil Gas*, *12*(7), 5–12.

Wolf, R. A., K. A. Farley, and L. T. Silver (1996), Helium diffusion and low temperature thermochronometry of apatite, *Geochim. Cosmochim. Acta*, *60*, 4231–4240, doi:10.1016/S0016-7037(96)00192-5.

Wood, D. J., and J. B. Saleeby (1997), Late Cretaceous-Paleocene extensional collapse and disaggregation of the southernmost Sierra Nevada batholith, *Int. Geol. Rev.*, *39*, 973–1009, doi:10.1080/00206819709465314.

Wood, P. R., and R. H. Dale (1964), Geology and ground-water features of the Edison-Maricopa are Kern County, California, *U.S. Geol. Surv. Water Supply Pap.*, *1656*, 101 pp.

Zandt, G., H. Gilbert, T. Owens, M. Ducea, J. Saleeby, and C. Jones (2004), Active foundering of a continental arc root beneath the southern Sierra Nevada, California, *Nature*, *431*, 41–45, doi:10.1038/nature02847.

K. A. Farley, J. Saleeby, and Z. Saleeby, Division of Geological and Planetary Sciences, California Institute of Technology, Pasadena, CA 91125, USA. (jason@gps.caltech.edu)

G. Mahéo, Laboratoire des Sciences de la Terre, Université de Lyon, Ecole Normale Supérieure de Lyon, Université Claude Bernard Lyon 1, UMR 5570 CNRS, Bat Géode, 43 Bd du 11 Novembre 1918, F-69622 Villeurbanne CEDEX, France. (gweltaz.maheo@univ-lyon1.fr)